

1 **Export fluxes in a naturally iron-fertilized area of the Southern
2 Ocean: importance of diatom resting spores and faecal pellets for
3 export (part 2).**

4 M. Rembauville^{1,2}, S. Blain^{1,2}, L. Armand³, B. Quéguiner⁴ and I. Salter^{1,2,5}

5 ¹ Sorbonne Universités, UPMC Univ Paris 06, UMR 7621, LOMIC, Observatoire Océanologique, Banyuls-sur-
6 Mer, France.

7
8 ² CNRS, UMR 7621, LOMIC, Observatoire Océanologique, Banyuls-sur-Mer, France.

9
10 ³ Department of Biological Sciences and Climate Futures, Macquarie University, New South Wales, Australia

11
12 ⁴ Aix-Marseille Université, Université de Toulon, CNRS/INSU, IRD, MOI, UM 110, Marseille, France.

13
14 ⁵ Alfred-Wegener-Institute for Polar and Marine research, Bremerhaven, Germany.

15
16 Correspondance to : M. Rembauville (rembauville@obs-banyuls.fr).

17

18

19 **Abstract**

20 The biological composition of the material exported to a moored sediment trap located
21 under the winter mixed layer of the naturally-fertilized Kerguelen Plateau in the Southern
22 Ocean was studied over an annual cycle. Despite iron availability in spring, the annual
23 particulate organic carbon (POC) export (98.2 mmol m⁻²) at 289 m was low but annual
24 biogenic silica export was significant (114 mmol m⁻²). This feature was related to the
25 abundance of empty diatom cells and the ratio of full:empty cells exerted a first order control
26 in BSi:POC export stoichiometry of the biological pump. *Chaetoceros Hyalochaete* spp. and
27 *Thalassiosira antarctica* resting spores were responsible for more than 60 % of the annual
28 POC flux that occurred during two very short export events of <14 days in spring-summer.
29 Relatively low diatom fluxes were observed over the remainder of the year. Faecal pellet
30 contribution to annual carbon flux was low (34 %) and reached its seasonal maximum in

31 autumn and winter (> 80 %). The seasonal progression of faecal pellet types revealed a clear
32 transition from small spherical shapes (small copepods) in spring, larger cylindrical and
33 ellipsoid shapes in summer (euphausiids and large copepods) and finally large tabular shapes
34 (salps) in autumn and winter. We propose in this High Biomass, Low Export (HBLE)
35 environment that small, but highly silicified and fast-sinking resting spores are able to bypass
36 the intense grazing pressure and efficient carbon transfer to higher trophic levels that are
37 responsible for the low fluxes observed the during the remainder of the year. More generally
38 our study also provides a statistical framework linking the ecological succession of diatom
39 and zooplankton communities to the seasonality of carbon and silicon export within an iron-
40 fertilized bloom region in the Southern Ocean.

41

42 **1 Introduction**

43 The Southern Ocean is the place of exposure of old upwelled waters to the atmosphere and
44 the formation of mode waters, thereby ventilating an important part of the global Ocean and
45 playing a central role in distributing heat, carbon and nutrients in the global Ocean (Sarmiento
46 et al., 2004; Takahashi et al., 2012; Sallée et al., 2012). Silicon trapping occurs in the
47 Southern Ocean because silicon is stripped out of the euphotic zone more efficiently than
48 phosphorous and nitrogen (Holzer et al., 2014). It is generally acknowledged that regional
49 variations in plankton community structure are responsible for variations in nutrient
50 stoichiometry in the Southern Ocean (Jin et al., 2006; Weber and Deutsch, 2010) and that the
51 biological pump is a central process regulating this stoichiometry (Ragueneau et al., 2006;
52 Salter et al., 2012; Primeau et al., 2013). These characteristics emphasize the importance of
53 biological processes in the Southern Ocean waters for the availability of silicic acid and
54 nitrate (Sarmiento et al., 2004; Dutkiewicz et al., 2005) as well as phosphate (Primeau et al.,
55 2013) at lower latitudes, thereby regulating part of the productivity of the global Ocean. It has
56 been proposed that change in the uptake ratio of silicate and nitrate by Southern Ocean
57 phytoplankton in response to increased iron availability during the Last Glacial Maximum
58 could have played a substantial role in varying atmospheric CO₂ (Brzezinski et al., 2002;
59 Matsumoto et al., 2002).

60 Primary production in the Southern Ocean is regulated by macro- and micronutrient
61 availability (Martin et al., 1990; Moore et al., 2001; Nelson et al., 2001; Moore et al., 2013)
62 and light-mixing regime (Venables and Moore, 2010; Blain et al., 2013). The complex
63 interaction of these factors introduces strong spatial heterogeneity in the distribution of
64 primary producer biomass (Arrigo et al., 1998; Thomalla et al., 2011). In particular, High
65 Nutrient, Low Chlorophyll (HNLC) areas in the open ocean contrast strongly with highly
66 productive, naturally fertilized, blooms located downstream of island systems such as the

67 Kerguelen Plateau (Blain et al., 2001, 2007), Crozet Islands (Pollard et al., 2002) and South
68 Georgia (Park et al., 2010; Tarling et al., 2012). The diatom-dominated phytoplankton blooms
69 characteristic of these island systems are the product of multiple environmental conditions
70 favorable for their rapid growth (Quéguiner, 2013), which appear to promote POC export
71 from the mixed layer (Nelson et al., 1995; Buesseler, 1998). However the ecological traits of
72 certain species can impact the BSi:POC export stoichiometry (Crawford, 1995; Salter et al.,
73 2012), and may therefore control the biogeochemical function of a particular region of the
74 Southern Ocean (Smetacek et al., 2004; Assmy et al., 2013)

75 Among the numerous ecological characteristics of plankton communities, algal
76 aggregation (Jackson et al., 2005; Burd and Jackson, 2009), mesozooplankton faecal pellets
77 (Lampitt et al., 1990; Wilson et al., 2008, 2013), vertical migrations of zooplankton and
78 mesopelagic fish (Jackson and Burd, 2001; Steinberg et al., 2002; Davison et al., 2013),
79 radiolarian faecal pellets (Lampitt et al., 2009), and diatom resting spore formation, (Salter et
80 al., 2012; Rynearson et al., 2013) have all been highlighted as efficient vectors of carbon
81 export out of the surface mixed layer. The challenge in describing the principal ecological
82 processes regulating POC export fluxes is the requirement to have direct access to sinking
83 particles. Many of the processes described occur in the upper layers of the ocean, where
84 circulation can strongly influence the reliability of sediment trap collections (Baker et al.,
85 1988; Buesseler et al., 2007). Short term deployments of free drifting sediment traps can be an
86 efficient solution to minimize the hydrodynamic bias (Buesseler et al., 2000; Lampitt et al.,
87 2008) but spatial and temporal decoupling of production and export needs to be considered
88 (Salter et al., 2007; Rynearson et al., 2013). In regions characterized by relatively weak
89 circulation, moored sediment trap observations in areas of naturally fertilized production can
90 track temporal succession of exported material from long-term (several month) blooms
91 (Westberry et al., 2013). Such an approach can partially resolve how ecological processes in

92 plankton communities regulate POC and biomineral export out of the mixed layer (Salter et
93 al., 2012; Salter et al., 2014), although selective processes during export may modify original
94 surface features

95 The central Kerguelen Plateau is a good environment to study the ecological vectors of
96 export with sediment traps due to the naturally fertilized recurrent bloom (Blain et al., 2007)
97 and shallow bathymetry that breaks the strong Antarctic Circumpolar Current flow (Park et
98 al., 2008, 2014). As reported in the companion paper (Rembauville et al., 2014), annual POC
99 export measured by the sediment trap deployment at 289 m beneath the southeastern iron-
100 fertilized Kerguelen bloom is $98 \pm 4 \text{ mmol m}^{-2} \text{ y}^{-1}$. This downward flux of carbon may account
101 for as little as $\sim 1.5 \text{ \%}$ of seasonal net community carbon production ($6.6 \pm 2.2 \text{ mol m}^{-2}$,
102 Jouandet et al., 2008) and $< 2 \text{ \%}$ of seasonally-integrated POC export estimated at 200 m from
103 a dissolved inorganic carbon budget (5.1 molC m^{-2} , Blain et al., 2007). Although
104 hydrodynamical and biological biases related to the shallow moored sediment trap
105 deployment may partly explain the low POC fluxes we report, independent measurements of
106 low POC fluxes ($> 300 \text{ m}$) at the same station (Ebersbach and Trull, 2008; Jouandet et al.,
107 2014) are consistent with the hypothesis of flux attenuation below the winter mixed layer.
108 These observations suggest a ‘High Biomass, Low Export’ (HBLE, Lam and Bishop, 2007)
109 status characterizing the productive Kerguelen Plateau. HBLE status appears to be a common
110 feature of other productive sites of the Southern Ocean (Lam and Bishop, 2007; Ebersbach et
111 al., 2011; Lam et al., 2011; Maiti et al., 2013; Cavan et al., 2015). Describing the temporal
112 succession of POC and BSi flux vectors from the Kerguelen Plateau is of interest to increase
113 our understanding of the ecological processes characterizing HBLE environments.

114 Numerous studies have described diatom fluxes from sediment trap records in the
115 Southern Ocean (Leventer and Dunbar, 1987; Fischer et al., 1988; Abelmann and Gersonde,
116 1991; Leventer, 1991; Gersonde and Zielinski, 2000; Fischer et al., 2002; Pilskaln et al.,

117 2004; Ichinomiya et al., 2008; Salter et al., 2012). Highest diatom fluxes recorded by
118 sediment traps ($>10^9$ valves $m^{-2} d^{-1}$) were observed in the Seasonal Ice Zone (SIZ) near
119 Prydz Bay and Adélie Land and were dominated by *Fragilariopsis kerguelensis* and smaller
120 *Fragilariopsis* species such as *Fragilariopsis curta* and *Fragilariopsis cylindrus* (Suzuki et
121 al., 2001; Pilskaln et al., 2004). These high fluxes occurred in summer and were associated
122 with the melting of sea ice. Changes in light availability and melt water input appear to
123 establish favorable conditions for the production and export of phytoplankton cells (Romero
124 and Armand, 2010). In the Permanently Open Ocean Zone (POOZ), highest diatom fluxes
125 recorded were two orders of magnitude lower $\sim 10^7$ valves $m^{-2} d^{-1}$ (Abelmann and Gersonde,
126 1991; Salter et al., 2012; Grigorov et al., 2014) and typically represented by *F. kerguelensis*
127 and *Thalassionema nitzschiooides*. One notable exception is the naturally iron-fertilized waters
128 downstream of the Crozet Plateau where resting spores of *Eucampia antarctica* var.
129 *antarctica* dominated the diatom export assemblage (Salter et al., 2012).

130 Other studies have reported faecal pellet contribution to POC fluxes in the Southern
131 Ocean (Dunbar, 1984; Wefer et al., 1988; Wefer et al., 1990; Wefer and Fisher, 1991;
132 Dubischar and Bathmann, 2002; Suzuki et al., 2001,2003; Accornero and Gowing, 2003;
133 Schnack-Schiel and Isla, 2005; Gleiber et al., 2012) with a particular emphasis on shelf
134 environments where faecal pellet contribution to POC flux was typically higher than in the
135 oceanic regions (Wefer et al., 1990; Wefer and Fischer, 1991; Schnack-Schiel and Isla, 2005).
136 In the Ross Sea, a northward decreasing contribution to carbon flux of 59 %, 38 % and 15 %
137 for southern, central and northern areas was reported from 235 m sediment traps deployments
138 (Schnack-Schiel and Isla, 2005). Faecal pellets in the Ross Sea were generally represented by
139 larger shapes with only 2 to 3 % of them present as small spherical or ellipsoid shapes and
140 total faecal pellet flux was slightly higher than 10^3 pellets $m^{-2} d^{-1}$. High faecal pellet
141 contribution to carbon fluxes (> 90 %) have been observed in the Bransfield Strait and the

142 Marginal Ice Zone of the Scotia Sea, and have been linked to the abundance of the Antarctic
143 krill *Euphausia superba*, resulting in maximum recorded fluxes of $>5 \times 10^5$ pellets $\text{m}^{-2} \text{ d}^{-1}$
144 (Bodungen, 1986; von Bodungen et al., 1987; Wefer et al., 1988). The strong contribution of
145 krill faecal pellets to carbon flux in the western Antarctic Peninsula was confirmed over
146 several years of observations, with the highest contributions to carbon flux succeeding the
147 phytoplankton bloom in January and February (Gleiber et al., 2012).

148 In the present study, particulate material exported from the mixed layer in the naturally
149 fertilized Permanently Open Ocean Zone (POOZ) of the Kerguelen Plateau is described from
150 an annual sediment trap mooring. To develop our understanding of seasonal variability in the
151 ecological flux vectors and particle biogeochemistry we investigate the link between the
152 chemical (POC, PON, BSi) and biological (diatom species and faecal pellet types)
153 components of exported particles. Furthermore, we advance the limitations of previous studies
154 by explicitly distinguishing full and empty diatom cells in the exported material and thereby
155 determine species-specific roles for carbon and silica export.

156 **2 Materials and methods**

157 As part of the multidisciplinary research program KEOPS2 a moored sediment trap
158 (Technicap PPS3) was deployed at 289 m (seafloor depth: 527 m) at the representative bloom
159 station A3 ($50^{\circ}38.3' \text{ S}$ – $72^{\circ}02.6' \text{ E}$) for a period of 321 days (21 October 2011 to 7
160 September 2012). The sediment trap mooring was located within an iron-fertilized bloom site
161 on the southern part of the Kerguelen Plateau (Blain et al., 2007). The cup rotation dates of
162 the sediment trap are listed in Table 1. Details of sediment trap design, hydrological
163 conditions, sample processing, POC and PON analyses and surface chlorophyll *a* data
164 extraction are described in a companion paper (Rembauville et al., 2014). Comparison with
165 thorium-based estimates of carbon export suggests a trapping efficiency of 15-30 % relative to

166 the proxy, although strong particle flux attenuation between 200 m and the trap depth (289 m)
167 might also contribute to the low fluxes. We therefore interpret our results to accurately reflect
168 the relationships between the biological and geochemical signals of the material caught by the
169 sediment trap, which we acknowledge may not necessarily represent the entire particle export
170 at 289 m.

171 **2.1 Biogenic and lithogenic silicon analyses**

172 For the analysis of biogenic silica (BSi) and lithogenic silica (LSi), 2 to 8 mg of freeze-dried
173 material were weighed (Sartorius precision balance, precision 10^{-4} g) and placed into falcon
174 tubes. The extraction of silicon from biogenic and lithogenic particle phases was performed
175 following the Ragueneau et al. (2005) triple NaOH/HF extraction procedure. Silicic acid
176 (Si(OH)_4) resulting from NaOH extractions was measured automatically on a Skalar 5100
177 autoanalyzer whereas Si(OH)_4 resulting from HF extraction was measured manually on a
178 Milton Roy Spectronic 401 spectrophotometer. Si(OH)_4 analyses were performed
179 colorimetrically following Aminot and Kerouel (2007). Standards for the analysis of samples
180 from the HF extraction were prepared in an HF/ H_3BO_4 matrix, ensuring the use of an
181 appropriate calibration factor that differs from Milli-Q water. The contribution of LSi to the
182 first leaching was determined by using Si:Al ratios from a second leaching step (Ragueneau et
183 al., 2005). Aluminum concentrations were measured by spectrophotometry (Howard et al.,
184 1986). The triple extraction procedure is optimized for samples with a BSi content $< 10 \mu\text{mol}$.
185 For some samples (cup #3, #4, #6, #7, #8, #9 and #10) the Si:Al molar ratio in the second
186 leachate was high (> 10) indicating the incomplete dissolution of BSi. For these samples it was
187 not possible to use Si:Al ratios to correct for LSi leaching. A crustal Si:Al mass ratio of 3.74
188 (Taylor and McClenan, 1986) was therefore used and applied to all the samples for
189 consistency. Precision (estimated from measurement of 25 independent samples) was 13
190 nmol/mg, which represents $< 1\%$ of the BSi content in all samples and 14 % of the mean LSi

191 content. Blank triplicates from each extraction were below the detection limit. BSi results
192 from this method were compared to the kinetic method from DeMaster (1981). There was an
193 excellent agreement between the two methods (Spearman rank correlation, $n = 12$, $p < 0.001$,
194 $BSi_{kinetic} = 1.03 BSi_{triple\ extraction} - 0.08$, data not shown). To estimate the contribution of opal
195 to total mass flux, we assumed an opal composition of $SiO_2 \cdot 0.4H_2O$ (Mortlock and Froelich,
196 1989).

197 In order to correct for the dissolution of BSi during deployment and storage, $Si(OH)_4$
198 excess was analyzed in the overlying preservative solution. Particulate BSi fluxes were
199 corrected for dissolution assuming that excess silicic acid originated only from the dissolution
200 of BSi phases. $Si(OH)_4$ excess was always $< 10\%$ of total (dissolved + particulate) Si
201 concentrations. Error propagation for POC, PON, BSi fluxes and molar ratios were calculated
202 as the quadratic sum of the relative error from triplicate measurements of each variable.

203 **2.2 Diatom identification, fluxes and biomass**

204 Many sediment trap studies reporting diatom fluxes in the Southern Ocean use a
205 micropaleontological protocol that oxidizes organic material ($KMnO_4$, HCl , H_2O_2) thereby
206 facilitating the observation of diatom valves (see Romero et al., 1999, 2000 for a description).
207 In the present manuscript, our specific aim was to separately enumerate full and empty diatom
208 cells captured by the sediment trap to identify key carbon or silicon exporters amongst the
209 diatom species. We therefore used a biological method following a similar protocol to that of
210 (Salter et al., 2007, 2012). To prepare samples for counting, 2 mL of a gently homogenized
211 1/8 wet aliquot were diluted in a total volume of 20 mL of artificial seawater ($S = 34$). In
212 order to minimize the exclusion and/or breaking of large or elongated diatom frustules (e.g.
213 *Thalassiothrix antarctica*), the pipette tip used for sub-sampling was modified to increase the
214 tip aperture to > 2 mm. The diluted and homogenized sample was placed in a Sedgewick-
215 Rafter counting chamber (Pyser SGE S52, 1 mL chamber volume). Each sample was

216 observed under an inverted microscope (Olympus IX71) with phase contrast at 200x and 400x
217 magnification. Diatom enumeration and identification was made from one quarter to one half
218 of the counting chamber (depending on cell abundance). The total number of diatoms counted
219 was >400 in all the cups with the exception of the winter cup #12 (May – September 2012)
220 where the diatom abundance was low (<100 diatoms counted). Diatoms species were
221 identified following the recommendations of Hasle and Syvertsen (1997). All whole, intact
222 and recognizable frustules were enumerated. Full and empty cells were counted separately,
223 following suggestions in Assmy et al. (2013).

224 Due to the lower magnification used and preserved cell contents sometimes obscuring
225 taxonomic features on the valve face, taxonomic identification to the species level was
226 occasionally difficult and necessitated the categorizing of diatom species to genus or taxa
227 groupings in the following manner: *Chaetoceros* species of the subgenus *Hyalochaete* resting
228 spores (CRS) were not differentiated into species or morphotypes but were counted separately
229 from the vegetative cells; *Fragilariopsis separanda* and *Fragilariopsis rhombica* were
230 grouped as *Fragilariopsis separanda/rhombica*; *Membraneis imposter* and *Membraneis*
231 *challengeri* and species of the genera *Banquisia* and *Manguinea* were denominated as
232 *Membraneis* spp. (Armand et al., 2008a); diatoms of the genus *Haslea* and *Pleurosigma* were
233 grouped as *Pleurosigma* spp.; all *Pseudo-nitzschia* species encountered were grouped as
234 *Pseudo-nitzschia* spp.; *Rhizosolenia antennata* and *Rhizosolenia styliformis* were grouped as
235 *Rhizosolenia antennata/styliformis*; large and rare *Thalassiosira oliverana* and *Thalassiosira*
236 *tumida* were grouped as *Thalassiosira* spp.; *Thalassiosira antarctica* resting spores (TRS)
237 were identified separately from the vegetative cells; small centric diatoms (<20 μm)
238 represented by *Thalassiosira gracilis* and other *Thalassiosira* species were designated as
239 Small centrics (< 20 μm); and finally large and rare centrics including *Azpeitia tabularis*,
240 *Coscinodiscus* spp. and *Actinocyclus curvatulus* were grouped as Large centrics (>20 μm).

241 Full and empty frustules of each species or taxa grouping were distinguished and enumerated
242 separately. The cell flux for each diatom species or taxa grouping was calculated according to
243 Equation (1):

244
$$Cell\ flux = N_{diat} \times d \times 8 \times V_{cup} \times \frac{1}{0.125} \times \frac{1}{days} \times chamber\ fraction \quad (1)$$

245 Where *Cell flux* is in valves $m^{-2} d^{-1}$, N_{diat} is the number of cells enumerated for each diatom
246 classification, d is the dilution factor from the original wet aliquot, 8 is the total number of
247 wet aliquots comprising one sample cup, V_{cup} is the volume of each wet aliquot, 0.125 is the
248 Technicap PPS/3 sediment trap collecting area (m^2), *days* is the collecting period, *chamber*
249 *fraction* is the surface fraction of the counting chamber that was observed (one quarter or one
250 half). The annually integrated full and empty diatom flux for each species was calculated
251 assuming as follows:

252

253
$$Annual\ flux_{(x)} = \sum_{i=1}^{12} (Flux_{(x)i} \times days_i) \quad (2)$$

254

255 Where *Annual flux_(x)* is the annually integrated flux of a full or empty diatom species x (cell
256 $m^{-2} y^{-1}$), $Flux_{(x)i}$ is the full or empty flux of this species in the cup number i (cell $m^{-2} d^{-1}$) and
257 $days_i$ is the collecting time for the cup number i (d). The calculations assume negligible export
258 occurred during the month of September which was not sampled by the sediment trap. We
259 consider this assumption reasonable based on the preceding flux profile and low concentration
260 of satellite-derived chlorophyll *a* (Rembauville et al. 2014).

261 We directly compared the micropaleontological (as used in Rigual-Hernández et al.
262 (2015)) and biological counting techniques in our sediment trap samples and noted the loss of
263 several species (*Chaetoceros decipiens*, *Chaetoceros dichaeta*, *Corethron pennatum*
264 *Corethron inerme*, *Guinardia cylindrus* and *Rhizosolenia chunii*) under the

265 micropaleontological technique. We attribute this to the aggressive chemical oxidation
266 techniques used to “clean” the samples as well as the centrifugation steps which may also
267 selectively destroy or dissolve certain frustules. For the species that were commonly observed
268 by both techniques, total valve flux was in good agreement (Spearman rank correlation, $n =$
269 12, $\rho = 0.91$, $p < 0.001$, data not shown) although consistently lower with the
270 micropaleontological technique, probably due to the loss of certain frustules described above.
271 Full details of this method comparison are in preparation for a separate submission.

272 Diatoms species that contributed to more than 1 % of total full cell flux were
273 converted to carbon flux. For *E. antarctica* var. *antarctica*, *Fragilariopsis kerguelensis*,
274 *Fragilariopsis separanda/rhombica*, *Pseudo-nitzschia* spp. and *Thalassionema nitzschiooides*
275 spp., we used published cell-specific carbon content ($Cell_C$, pgC cell $^{-1}$) for diatoms
276 communities of the Kerguelen Plateau from Cornet-Barthaux et al. (2007). As *Chaetoceros*
277 *Hyalochaete* resting spores (CRS) and *Thalassiosira antarctica* resting spores (TRS) largely
278 dominated the full diatom fluxes (>80%), an appropriate estimation of their carbon content
279 based on the specific sizes observed in our dataset was required for accurate quantification of
280 their contribution to carbon fluxes. Biomass calculations for both CRS and TRS were
281 determined from >50 randomly selected complete resting spores observed in splits from cups
282 #4 to #11 (December 2011 to May 2012). Morphometric measurements (pervalvar and apical
283 axis) were made using the Fiji image processing package (available at <http://fiji.sc/Fiji>) on
284 images taken with an Olympus DP71 camera. Cell volumes followed appropriate shape
285 designated calculations from Hillebrand et al. (1999) (Table 2). The cell volume coefficient of
286 variation was 46 % and 54 % for CRS and TRS, respectively. CRS carbon content was
287 estimated from the derived cell volume using the volume to carbon relationship of 0.039
288 pmolC μm^3 established from the resting spore of *Chaetoceros pseudocurvisetus* (Kuwata et
289 al., 1993), leading to a mean $Cell_C$ value of 227 pgC cell $^{-1}$ (Table 2). There is currently no

290 volume to carbon relationship for *Thalassiosira antarctica* resting spores described in the
291 literature, therefore, the allometric relationship for vegetative diatoms (Menden-Deuer and
292 Lessard, 2000) was used to calculate our TRS carbon content, giving a mean $Cell_C$ value of
293 1428 pgC cell $^{-1}$ (Table 2). Full diatom fluxes were converted to carbon fluxes as follows:

294

$$C\ flux_{(x)} = \frac{Flux_{(x)} \times Cell_{C(x)}}{M_{12C} \times 10^9} \quad (3)$$

295 where $C\ flux_{(x)}$ is the carbon flux carried by each diatom species x (mmol C m $^{-2}$ d $^{-1}$), $Flux_{(x)}$ is
296 the full cell numerical flux of species x (cell m $^{-2}$ d $^{-1}$), $Cell_{C(x)}$ is the carbon content of species x
297 (pgC cell $^{-1}$) and M_{12C} is the molecular weight of ^{12}C (12 g mol $^{-1}$) and 10^9 is a conversion factor
298 from pmol to mmol.

299

2.3 Faecal pellet composition and fluxes

300 To enumerate faecal pellets an entire 1/8 aliquot of each sample cup was placed in a gridded
301 petri dish and observed under a stereomicroscope (Zeiss Discovery V20) coupled to a camera
302 (Zeiss Axiocam ERc5s) at 10x magnification. Photographic images (2560 x 1920 pixels, 3.49
303 $\mu\text{m pixel}^{-1}$) covering the entire surface of the petri dish were acquired. Following Wilson et al.
304 (2013), faecal pellets were classified into five types according to their shape: spherical, ovoid,
305 cylindrical, ellipsoid and tabular. The flux of each faecal pellet class (nb m $^{-2}$ d $^{-1}$) was
306 calculated as follows:

307

$$Faecal\ pellet\ flux = N_{FP} \times 8 \times \frac{1}{0.125} \times \frac{1}{days} \quad (4)$$

308 where N_{FP} is the number of pellets within each class observed in the 1/8th aliquot. The other
309 constants are as described in Eq. (1). Individual measurements of the major and minor axis for
310 each faecal pellet were performed with the Fiji software. The total number of spherical, ovoid,
311 cylindrical, ellipsoid and tabular faecal pellets measured was 4041, 2047, 1338, 54 and 29,

312 respectively. Using these dimensions, faecal pellet volume was determined using the
313 appropriate shape equation (e.g. sphere, ellipse, cylinder, ovoid/ellipse) and converted to
314 carbon using a factor of 0.036 mgC mm⁻³ (Gonzalez and Smetacek, 1994). Due to the
315 irregularity of the tabular shapes preventing the use of single equation to calculate their
316 volume, a constant value of 119 µgC pellet⁻¹ representing a midrange value for tabular shapes
317 (Madin, 1982), was applied to tabular faecal pellets (Wilson et al., 2013). This value was
318 appropriate because the observed tabular faecal pellets were within the size range reported in
319 Madin (1982). Ranges and mean values of faecal pellet volumes and carbon content are
320 reported in Table 3. Faecal fluff and disaggregated faecal pellets were not considered in these
321 calculations because quantitative determination of their volume is difficult. We acknowledge
322 that fragmentation of larger pellets may represent an artifact of the sample splitting procedure.
323 Alternatively, their presence may also result from natural processes within the water column,
324 although dedicated sampling techniques (e.g. polyacrylamide gel traps) are required to make
325 this distinction (Ebersbach et al., 2014, 2011; Ebersbach and Trull, 2008; Laurenceau et al.,
326 2014). Consequently our present quantification of faecal pellet carbon flux should be
327 considered as lower-end estimates.

328 The precision of our calculations depends on the reliability of carbon-volume
329 conversion factors of faecal pellets, which vary widely in the literature, as well as variability
330 in diatom resting spore volumes (Table 2). To constrain the importance of this variability on
331 our quantitative estimation of C flux, we calculated upper and lower error bounds by a
332 constant scaling of the conversion factors ($\pm 50\%$).

333 2.4 Statistical analyses

334 Correspondence analysis was performed to summarize the seasonality of diatom export
335 assemblages. This approach projects the original variables (here full and empty cells) onto a

336 few principal axes that concentrate the information of the Chi-squared (Chi^2) distance
337 between both observations and variables (Legendre and Legendre, 1998). Chi^2 distance is
338 very sensitive to rare events. Consequently, only species with an annual mean flux higher than
339 10% of the mean annually integrated flux of all the species were retained in the
340 correspondence analysis. This selection was performed separately on full and empty cell
341 fluxes.

342 Partial least square regression (PLSR) analysis was used to examine the relationships
343 between ecological flux vectors (full and empty diatom cells and faecal pellet fluxes as
344 columns of the X matrix, cups being the rows) and bulk geochemical properties (POC flux,
345 PON flux, BSi flux, POC:PON and BSi:POC molar ratio and columns in the Y matrix) of the
346 exported material. The principle of PLSR is to decompose both the X and Y matrix into their
347 principal components using principal component analysis and then use these principal
348 components to regress Y in X (Abdi, 2010). PLSR is capable of modeling response variables
349 from a large set of predictors. The same filter as for the correspondence analysis (full- and
350 empty -cell fluxes $>10\%$ of the total mean flux) was applied.

351 **3 Results**

352 **3.1 Chemical composition of the settling material**

353 Time series of the chemical signature of the settling material are presented in Fig. 1
354 and export fluxes are reported in Table 1. POC and PON fluxes are already reported and
355 discussed in the companion paper (Rembauville et al., 2014). BSi fluxes exhibited the same
356 seasonal pattern as POC fluxes (Fig. 1c) with low fluxes ($< 1 \text{ mmol m}^{-2} \text{ d}^{-1}$) except during the
357 two intense events (2.60 ± 0.03 and $2.19 \pm 0.10 \text{ mmol m}^{-2} \text{ d}^{-1}$, mean \pm standard deviation).
358 LSi fluxes were highest in in spring ($>10 \text{ } \mu\text{mol m}^{-2} \text{ d}^{-1}$ in cups #1 to #4, October to December
359 2011, Table 1). The contribution of LSi to total particulate Si was 5 % and 10 % respectively

360 in cups #1 (October/November 2011) and #12 (May to September 2012) and lower than 3 %
361 the remainder of the year. The BSi:POC molar ratio was highest at the beginning of the
362 season (between 2.18 ± 0.19 and 3.46 ± 0.16 in the first three cups from October to December
363 2011, blue line in Fig. 1c) and dropped to 0.64 ± 0.06 in cup #5 (end December 2011),
364 following the first export event. BSi:POC ratios were close in the two export events ($1.62 \pm$
365 0.05 and 1.49 ± 0.08). The lowest BSi:POC ratio was observed in autumn in cup #11 ($0.29 \pm$
366 0.01 , February to May 2012). Similarly, the opal contribution to total mass flux was highest in
367 spring (70.8 % in cup #2, November 2011) and lowest in autumn (21.5 % in cup #11,
368 February to May 2012).

369 **3.2 Diatom fluxes**

370 Diatoms from 33 taxa were identified and their fluxes determined across the 11-months time
371 series. Fluxes are reported in Table 4 and Table 5 for full and empty cells, respectively. Full
372 and empty cell fluxes for the total community and for the taxa that are the major contributors
373 to total diatom flux (eight taxa that account for >1 % of total cells annual export) are
374 presented in Fig. 2. The full and empty cell fluxes for each diatom species or taxa are reported
375 in Table 4 and 5, respectively.

376 During spring (cups #1 to #3, October to December 2011) and autumn/winter (cups
377 #11 and #12, February to September 2012) the total flux of full cells was $< 5 \times 10^6$ cells $m^{-2} d^{-1}$
378 (Fig. 2a). The total flux of full cells increased to 5.5 and 9.5×10^7 cells $m^{-2} d^{-1}$ (cups #4 and
379 #9, December and end January respectively) during two episodic (<14 days) sedimentation
380 events. The two largest flux events (cups #4 and #9) were also associated with significant
381 export of empty cells with respectively 6.1×10^7 and 2.9×10^7 cells $m^{-2} d^{-1}$ (Fig. 2a). For
382 *Chaetoceros Hyalochaete* spp. resting spores (CRS), full cells fluxes of 4×10^7 cells $m^{-2} d^{-1}$
383 and 7.8×10^7 cells $m^{-2} d^{-1}$ accounted for 76 % and 83 % of the total full cell flux during these

384 two events, respectively (Fig. 2b), whereas a smaller contribution of *Thalassiosira antarctica*
385 resting spores (TRS) (2.7×10^6 cells $m^{-2} d^{-1}$, 5 % of total full cells) was observed during the
386 first event (Fig. 2h). CRS also dominated (79-94 %) the composition of full cells in the
387 intervening period (cups #5-#8, December 2011 to January 2012), although the magnitude of
388 cell flux was moderate ($9 \times 10^6 - 2.5 \times 10^7$ cells $m^{-2} d^{-1}$) by comparison (Fig. 2b). In cup #4
389 (December 2011), the empty cell flux contained 61 % of *C. Hyalochaete* spp. vegetative
390 empty cells and 27 % of unidentified Small centrics (<20 μm) empty cells. In cup #9 (end
391 January 2012), the total empty cells flux contained 60 % of *C. Hyalochaete* spp. vegetative
392 stage and only 2 % of Small centrics (<20 μm) empty cells.

393 *Fragilariopsis kerguelensis*, and *Fragilariopsis separanda/rhombica* (Fig. 2d and 2e)
394 were mostly exported from spring through the end of summer (cups #1 to #10, October 2011
395 to February 2012) with total (full + empty) fluxes $< 3 \times 10^6$ cells $m^{-2} d^{-1}$, a value ~20 times
396 lower than the highest CRS fluxes recorded. During this time, these species were represented
397 by >50 % of empty cells. In autumn and winter, (cups #10 and #11, February to May 2012),
398 these species were only represented by low fluxes ($< 0.5 \times 10^6$ cells $m^{-2} d^{-1}$) of empty cells.
399 *Thalassionema nitzschiooides* spp. fluxes were highest in spring and early summer (cups #1 to
400 #4, October to December 2011) with total fluxes comprised between 3.5×10^6 and 6.7×10^6
401 cells $m^{-2} d^{-1}$ (Fig. 2g). The remainder of the year, total flux was $< 2 \times 10^6$ cells $m^{-2} d^{-1}$ and was
402 essentially represented by full cells. *Pseudo-nitzschia* spp. were mostly represented by full
403 cells (Fig. 2f) with the highest flux of 1.2×10^7 cells $m^{-2} d^{-1}$ observed in the second intense
404 export event (cup #9, end January 2012). *Eucampia antarctica* var. *antarctica* total fluxes
405 were always represented by >50 % of full cells (Fig. 2c). Total cell fluxes of *Eucampia*
406 var. *antarctica* gradually increased from $< 1 \times 10^5$ to 1.3×10^6 cells $m^{-2} d^{-1}$ from
407 spring to summer (cups #1 to #9, October 2011 to January 2012) and then decreased to a
408 negligible flux in winter (cup #12, May to September 2012). This species was observed as

409 both the lightly silicified, chain-forming, vegetative form and the highly silicified winter
410 growth stage form. Both forms were observed throughout the year without specific seasonal
411 pattern. Small centric species ($<20 \mu\text{m}$) were essentially represented by empty cells (Fig. 2i).
412 Their total fluxes were $<4 \times 10^6 \text{ cells m}^{-2} \text{ d}^{-1}$, except in the first export event (cup #4,
413 December 2011) where their flux represented a considerable export of $1.7 \times 10^7 \text{ cells m}^{-2} \text{ d}^{-1}$.

414 Diatoms and sampling cup projection on the first two axes from the correspondence
415 analysis is presented in Fig. 3. Chi² distance in the correspondence analysis is based on
416 frequency distribution, therefore the results of the analysis must be considered as
417 representative of the community composition as opposed to cell flux. The first two factors
418 accounted for the majority (75.6 %) of total explained variance. Early in the season (cups #1-
419 #3, October to mid-December 2011), during the period of biomass accumulation in the
420 surface (Fig 1a), diatom fluxes were characterized by empty cells of *T. nitzschioides* spp. and
421 *F. kerguelensis*. Full TRS cells were observed in cup #3 (end November 2011) following the
422 initial bloom decline. The first major flux event (cup #4, December 2011) contained mostly
423 TRS, empty Small centrics ($< 20 \mu\text{m}$) cells and empty *C. Hyalochaete* spp. cells. The summer
424 flux period (cups #5 to #8, December 2011 to January 2012) primarily consisted of CRS,
425 although *E. antarctica* var. *antarctica*, *Pseudo-nitzschia* spp., and *Thalassiothrix antarctica*
426 were present as full cells and *Plagiotropis* spp., *Membraneis* spp., *Pseudo-nitzschia* spp. as
427 empty cells. The second major flux event (cup #9, end January 2012) was tightly associated
428 with CRS and full *Pseudo-nitzschia* spp. cells. Subsequent cups (#10 and #11, February to
429 May 2012) were characterized by full cells of *E. antarctica* var. *antarctica* and *Thalassiothrix*
430 *antarctica* and empty cells of *Corethron inerme*, *P. alata*, *F. separanda/rhombica* and *F.*
431 *kerguelensis*. Winter fluxes (cup #12, May to September 2012) were similar to the initial three
432 cups characterized primarily by empty cells of small diatom taxa. The centralized projection

433 in Fig. 3 of full *F. kerguelensis* and *T. nitzschiooides* spp. highlights their constant presence
434 throughout the annual record.

435 The total empty:full cell ratio is presented in Fig. 2a (blue line). This ratio was highest
436 in spring and early summer (cups #1 to #4, October to December 2011), ranging between 1.1
437 and 2.4, suggesting more empty cells to full cells. The ratio was lowest, representing
438 considerably more full cells to empty cells in cups #5 to #10 (December 2011 to February
439 2012) with values between 0.1 and 0.4. In autumn (cup #11, February to May 2012), the
440 empty:full ratio increased to 0.7. In the winter cup #12 (May to September 2012), the total
441 amount of full diatom cells was very low and therefore we could not calculate a robust
442 empty:full ratio. Across the time-series certain diatom taxa were observed exclusively as
443 empty cells, notably *Chaetoceros atlanticus* f. *bulbosum*, and *Corethron pennatum*. For
444 diatom taxa present as full and empty cells we calculated an annually integrated empty:full
445 ratio (Fig. 4) and arbitrarily defined threshold values of 2 (representing species mainly
446 observed as empty cells) and 0.5 (representing species mainly observed as full cells),
447 respectively. In decreasing order, the diatom taxa exhibiting empty:full ratios >2 were
448 *Thalassiosira lentiginosa*, Small centrics ($<20 \mu\text{m}$), *Proboscia alata*, *Rhizosolenia*
449 *antennata/styliformis*, *Chaetoceros decipiens*, *Corethron inerme*, *Dactyliosolen antarcticus*,
450 Large centrics ($>20 \mu\text{m}$), and *Asteromphalus* spp. The diatom taxa displaying an empty:full
451 ratio <0.5 were *Thalassiothrix antarctica*, *Rhizosolenia simplex*, CRS, *Eucampia antarctica*
452 var. *antarctica*, *Thalassiosira* spp. and *Navicula* spp. Species or grouped taxa with ratio
453 values falling between the thresholds <2 and >0.5 (*R. chunii*, through to *C. dichaeta* in Fig. 4)
454 were perceived as being almost equally represented by full and empty cells when integrated
455 annually across the time series.

456 **3.3 Faecal pellet fluxes**

457 The seasonal flux of faecal pellet type, volume and their estimated carbon flux are
458 summarized in Fig. 5 and Table 6. Total faecal pellet flux was $<2 \times 10^3$ pellets $\text{m}^{-2} \text{ d}^{-1}$ in
459 spring (cups #1 to #3, October to December 2011). Cups #4 and #5 (December 2011) were
460 characterized by the highest fluxes of 21.8×10^3 and 5.1×10^3 pellets $\text{m}^{-2} \text{ d}^{-1}$ (Fig. 5a, Table
461 6). Faecal pellet numerical flux decreased gradually from mid-summer (cup #5, December
462 2011) to reach a minimal value in winter (140 pellets $\text{m}^{-2} \text{ d}^{-1}$ in cup #12, May to September
463 2012). In spring (cups #1 to #3, October to December 2011), spherical and cylindrical shapes
464 dominated the numerical faecal pellet fluxes. Ellipsoid and tabular shapes were absent from
465 these spring cups. The first export event (cup #4, December 2011), was numerically
466 dominated by the spherical shaped pellets, however the remainder of the summer (cups #5 to
467 #10, December 2011 to February 2012) contained spherical, ovoid and cylindrical shapes in
468 comparable proportions. Ellipsoid shapes were observed from mid-summer to autumn (cups
469 #7 to #11, January to May 2012) but their overall contribution to pellet flux was low ($<6\%$,
470 Table 6). Rare tabular shapes were observed in summer (cups #6 and #8, December and
471 January 2012) and their contribution to numerical fluxes was highest in autumn and winter
472 (cups #11 and #12, February to September 2012).

473 The median faecal pellet volume showed a seasonal signal with a maximum peak >5.5
474 $\times 10^6 \mu\text{m}^3$ in mid-summer (cups # 6 to #8, mid-December to January 2012) and values $<4 \times$
475 $10^6 \mu\text{m}^3$ the remainder of the year (Fig. 5b). Concomitantly with the highest median volume,
476 the largest variance in faecal pellet size was also observed in the summer (highest
477 interquartile values in Fig. 5b).

478 Total faecal pellet carbon flux was lowest in spring ($<0.05 \text{ mmolC m}^{-2} \text{ d}^{-1}$ in cups #1
479 to #3, October to December 2011, Fig. 5c, Table 6). The highest total faecal pellet carbon flux
480 of nearly $0.5 \text{ mmolC m}^{-2} \text{ d}^{-1}$ was observed during the first export event in cup #4 (December
481 2011) and was essentially composed of spherical shapes (83 %, Table 6). For the remainder of

482 the summer (cups #5 to #10, December 2011 to February 2012), total faecal pellet carbon flux
483 was between 0.03 and 0.15 mmolC m⁻² d⁻¹ with a dominant contribution of cylindrical,
484 ellipsoid and tabular shapes. In autumn and winter (cups #11 and #12, February to September
485 2012), faecal pellet carbon fluxes of 0.13 and 0.06 mmolC m⁻² d⁻¹ were strictly dominated by
486 tabular shapes (>90 % to total faecal pellet carbon fluxes, Table 6).

487 **3.4 Statistical analysis of biological and biogeochemical signatures**

488 The β correlation coefficients of standardized variables obtained from the PLSR
489 analysis are presented as a heatmap in Fig. 6. The full cell fluxes of all diatom taxa, in
490 addition to spherical and ovoid and ellipsoid faecal pellet fluxes were positively correlated to
491 POC and PON fluxes. By contrast, empty cell fluxes of *F. kerguelensis*, *P. alata*, *T.*
492 *nitzschiooides* spp., *T. lentiginosa* and cylindrical, ellipsoid and tabular pellet fluxes were
493 either uncorrelated or negatively correlated with POC and PON fluxes. Full- and empty-cell
494 fluxes of all diatom taxa were positively correlated with BSi fluxes, although this correlation
495 was notably weak for empty cells of *C. inerme*, *P. alata* and *T. lentiginosa*. Only spherical
496 and ovoid faecal pellets were positively correlated with BSi fluxes. Full cells fluxes of CRS
497 and *E. antarctica* var. *antarctica* were the most negatively correlated with BSi:POC molar
498 ratio, whereas TRS, *F. kerguelensis*, *T. nitzschiooides* spp. and *T. lentiginosa* full cells fluxes
499 were positively correlated. Spherical and ovoid faecal pellets were weakly and negatively
500 correlated with the BSi:POC molar ratio whereas the cylindrical, ellipsoid and tabular shapes
501 were more strongly negatively correlated to the BSi:POC molar ratio. All the biological
502 components exhibited weak or no correlations to the POC:PON molar ratio.

503 The first two latent vectors of the PLSR accounted for 61.3 % and 74.1 % of
504 cumulative variance in X (full and empty diatom and pellet fluxes) and Y (biogeochemical
505 properties). In order to visualize how the seasonal succession of flux vectors was related to

506 the bulk geochemical properties of particles, the sampling cups, biological and chemical
507 factors were projected on the first two latent factors of the PLSR analysis (Fig. 7). Positively
508 projected on the first axis are the POC, PON and BSi fluxes, close to the export events
509 sampled in cups #4 (December 2011) and #9 (end January 2012). The closest biological
510 components comprise a complex assemblage of full and empty cells and spherical and ovoid
511 faecal pellet shapes. All the other cups are projected far from these two export events. The
512 second axis opposes the spring cups (#1 to #3, October to mid-December 2011) to the autumn
513 (#11, February to May 2012) and winter (#12, May to September 2012) cups. Empty frustules
514 of *F. kerguelensis*, *T. lentiginosa* and *T. nitzschiooides* spp. are projected close to the spring
515 cups (#1 to #3, October to mid-December 2011) together with the BSi:POC molar ratio
516 whereas autumn (#11, February to May 2012) and winter cups (#12, May to September 2012)
517 are projected far from the BSi:POC molar ratio and close to the tabular and cylindrical faecal
518 pellet shapes.

519 **3.5 Partitioning carbon fluxes among ecological vectors**

520 We estimated the contribution of resting spores and faecal pellets to carbon flux, calculated
521 their cumulative values and compared them to measured values (Fig. 8a and 8b). A highly
522 significant correlation (Spearman rank correlation, $n= 36$, $\rho = 0.84$, $p <0.001$) was evident
523 between calculated and measured carbon flux suggesting that the main ecological flux vectors
524 observed in the sample were capable of explaining the seasonal variation in total POC flux.
525 Table 7 lists the contribution of each vector to the calculated flux. In cup #1 (October to mid-
526 November 2011), CRS and other diatoms dominated the calculated POC fluxes, with
527 respectively 25.3 % and 38.6 %. Diatoms other than spores dominated the calculated carbon
528 flux (35.4 %) together with cylindrical faecal pellets (36.4 %) in cup #2 (November 2011).
529 TRS dominated the POC fluxes (85.1 %) in cup #3 (November/December 2011). CRS strictly
530 dominated the calculated POC fluxes in summer (cups #4 to #10, December 2011 to February

531 2012) with a contribution ranging from 46.8 % to 88.1 %. During the autumn and winter
532 (cups #11 and #12, February to September 2012), POC fluxes were almost exclusively
533 associated to tabular faecal pellets, 81 % and 93.3 %, respectively. At annual scale diatoms
534 resting spores (CRS and TRS), other diatoms and faecal pellets respectively accounted for
535 60.7 %, 5 % and 34.3 % of the calculated POC fluxes. Annual POC fluxes estimated from
536 ecological vectors considered here were slightly less than measured values (93.1 versus 98.2
537 mmol m⁻²).

538 **4 Discussion**

539 **4.1 The significance of resting spores for POC flux**

540 Generally POC fluxes were <0.5 mmol m⁻² d⁻¹ with the notable exception of two pulsed (<14
541 days) export events of ~1.5 mmol m⁻² d⁻¹ that accounted for ~40 % of annual POC export.
542 These two flux events were characterized by a noticeable increase and general dominance of
543 diatom resting spores. During both of these pulsed export events, cumulative *Chaetoceros*
544 *Hyalochaete* spp. resting spores (CRS) and *Thalassiosira antarctica* resting spores (TRS)
545 fluxes accounted for 66 % and 88 % of the measured POC flux, whereas total faecal pellet
546 flux accounted for 29 % and 5.2 %, respectively (Table 7). The combination of CRS and TRS
547 were responsible for 60.7 % of the annual calculated POC flux, a value ten times higher than
548 the contribution of other diatoms (5 %). We did not observe any full cells of the vegetative
549 stage of *Chaetoceros Hyalochaete*, a feature possibly related to its high susceptibility to
550 grazing pressure in the mixed layer (Smetacek et al., 2004; Quéguiner, 2013; Assmy et al.,
551 2013). Empty *Chaetoceros Hyalochaete* spp. cells were vegetative stages different in shape
552 from the resting spores. These empty frustules may be the remnants of vegetative stages
553 following spore formation. Alternatively, dissolution of the lightly silicified valves or girdle
554 bands of the vegetative cell could result in the rapid consumption of the cellular organic

555 material in the upper water column and this may also explain the absence of full vegetative
556 cells in the sediment trap record. Our flux data reveal that small (10 to 30 μm) and highly
557 silicified resting spores bypass the intense grazing pressure characterizing the base of the
558 mixed layer, and are the primary mechanism through which carbon and, to a lesser extent
559 silicon, is exported from the surface.

560 Numerous sediment trap studies have reported a strong contribution, if not dominance,
561 of CRS to diatom fluxes at depth in various oceanographic regions: firstly, in coastal
562 influenced regions (e.g. Antarctic Peninsula (Leventer, 1991), Bransfield Strait (Abelmann
563 and Gersonde, 1991), Gulf of California (Sancetta, 1995), the Omura Bay (Kato et al., 2003),
564 Santa Barbara basin (Lange, 1997), North Pacific Ocean (Chang et al., 2013) and the Arctic
565 (Onodera et al., 2014)), secondly in upwelling-influenced regions (Eastern Equatorial Atlantic
566 (Treppke et al., 1996)) and finally in the open ocean in the subarctic Atlantic (Rynearson et
567 al., 2013). Similar to sediment trap observations, CRS are reported as dominant in surface
568 sediments of coastal regions (peri-Antarctic shelf and Antarctic sea ice (Crosta et al., 1997;
569 Zielinski and Gersonde, 1997; Armand et al., 2005), the North Scotia Sea (Allen et al., 2005)
570 and east of Kerguelen Island (Armand et al., 2008b)), but also in upwelling-influenced
571 regions (the northeastern Pacific (Grimm et al., 1996), the northeast Pacific (Lopes et al.,
572 2006)) and finally in the open ocean (the North Atlantic, Bao et al., 2000). Moreover, the
573 annual POC export from the A3 station sediment trap at 289 m ($98.2 \pm 4.4 \text{ mmol m}^{-2} \text{ y}^{-1}$) falls
574 near annual estimates from deep sediment traps (>2000 m) located in the naturally fertilized
575 area downstream of the Crozet Islands ($37-60$ and $40-42 \text{ mmol m}^{-2} \text{ y}^{-1}$, Salter et al., 2012)
576 where fluxes were considered as mainly driven by resting spores of *Eucampia antarctica* var.
577 *antarctica*. Diatom resting spores are frequently observed in blooms heavily influenced by the
578 proximity of the coast. Major resting spores contribution to carbon fluxes was observed in
579 only one study in the open North Atlantic Ocean (Rynearson et al., 2013), but they are

580 generally absent or very rare in open ocean sediment trap studies (Fischer et al., 2002;
581 Grigorov et al., 2014; Rigual-Hernández et al., 2015). The frequent occurrence and
582 widespread distribution of diatoms resting spores in the neritic or coastal-influenced ocean
583 suggest their pivotal role in the efficient transfer of carbon to depth in these areas.

584 *Chaetoceros* resting spores have been reported to contain up to 10 times more carbon
585 than the vegetative forms (Kuwata et al., 1993) with no vacuole and high contents of lipids
586 and carbohydrates (Doucette and Fryxell, 1983; Kuwata et al., 1993). Moreover, CRS resist
587 grazing and have been found to lower copepods grazing pressure (Kuwata and Tsuda, 2005).
588 We suggest that diatom resting spores gather three essential characteristics for effective POC
589 export to the deep ocean: (1) they efficiently bypass the grazing pressure near the mixed layer
590 due to their morphological characteristics such as very robust frustules (CRS) or numerous
591 spines (TRS) (high export efficiency), (2) they are efficiently transferred to depth due to the
592 thick and dense frustule increasing sinking velocity and (3) their high carbon content is
593 protected from microbial degradation by the thick frustules (these last two points result in a
594 high transfer efficiency). The spatial distribution and formation of resting spores may
595 therefore be an integral ecological component defining the strength and efficiency of the
596 biological pump in specific regions. Nutrient depletion has been shown to trigger resting spore
597 formation in *Chaetoceros Hyalochaete* laboratory cultures (Garrison, 1981; Sanders and
598 Cibik, 1985; Kuwata et al., 1993; Oku and Kamatani, 1997) over relatively rapid timescales
599 (6 to 48 h, McQuoid and Hobson, 1996). Although Si(OH)₄ depletion appears to be the most
600 likely biogeochemical trigger at the Kerguelen Plateau (from 24 $\mu\text{mol L}^{-1}$ in early spring to 2
601 $\mu\text{mol L}^{-1}$ in summer, (Mosseri et al., 2008; Closset et al., 2014)), other environmental factors
602 (iron or light availability) could influence resting spore formation. Notably, dissolved iron
603 concentration in the mixed layer rapidly decreases to 0.1~0.2 nmol L^{-1} after the beginning of
604 the spring bloom at A3, however the vertical entrainment is much weaker in summer

605 compared to spring (Bowie et al., 2014). Rynearson et al. (2013) reported the absence of
606 spores in the mixed layer despite a strict dominance into the trap samples. A resting spore
607 formation at some depth (possibly implying a light control) would explain the temporal
608 decoupling between the surface production tracked by the satellite in the surface layer (first
609 ~20 meters) and the export events. Further work to establish seasonal dynamics of factors
610 linked to diatom life cycles and specifically the formation of resting spore is necessary.

611 **4.2 Contribution of faecal pellets to POC flux**

612 Although diatom resting spores are the primary vector for POC flux below the mixed
613 layer, faecal pellets were also important and accounted for 34.3 % of annual export. It has
614 been hypothesized that faecal pellets are the dominant flux component in High Biomass, Low
615 Export (HBLE) environments, where biomass is routed to higher trophic levels (Lam and
616 Bishop, 2007; Ebersbach et al., 2011). However, this hypothesis does not appear to be true for
617 the bloom of the central Kerguelen Plateau suggesting that faecal material is efficiently
618 reprocessed in the mixed layer, or that a significant part of the pellet flux is excreted below
619 the trap depth by vertically migrating zooplankton. Small spherical faecal pellets dominated
620 the annual numerical faecal pellet flux (53.8 %, Table 6). The short and intense export of
621 small spherical faecal pellets was concomitant with the first strong POC export in cup #4
622 (December 2011, Table 6). The significance of small spherical faecal pellets to POC flux is
623 somewhat uncharacteristic in comparison to other sediment trap records in shallow areas of
624 the Southern Ocean (Schnack-Schiel and Isla, 2005). They are possibly produced by small
625 cyclopoid copepods, like *Oithona similis* that are abundant in the POOZ (Fransz and
626 Gonzalez, 1995; Pinkerton et al., 2010). More specifically, *O. similis* represents >50 % of
627 mesozooplankton abundance at A3 in spring (Carlotti et al., 2015) has been observed at
628 station A3 in summer (Carlotti et al., 2008). *Oithona* species are known to be coprophagous
629 and play an important role in flux reprocessing (Gonzalez and Smetacek, 1994), which may

630 partially contribute to the rapid flux attenuation observed by efficiently retaining carbon in the
631 mixed layer. This reprocessing feeding strategy might also explain the low faecal pellet flux
632 we observed (highest value of 21.8×10^3 pellet $m^{-2} d^{-1}$), which was two orders of magnitude
633 lower than the $>5 \times 10^5$ pellet $m^{-2} d^{-1}$ observed in neritic areas where euphausiids dominate
634 the mesozooplankton community (Bodungen, 1986; von Bodungen et al., 1987; Wefer et al.,
635 1988).

636 There were notable differences in faecal pellet type over the course of the season. The
637 transition from spherical and ovoid pellets in spring to larger cylindrical and tabular pellets in
638 summer presumably reflects shifts in dominant zooplankton species from small cyclopoid
639 copepods towards larger calanoid copepods, euphausiids and salps (e.g. Wilson et al., 2013).
640 Carlotti et al. (2015) report that mesozooplankton biomass doubled between October and
641 November 2011 and was three-fold higher in January 2005 (Carlotti et al., 2008). In spring,
642 Carlotti et al. (2015) observed that the small size fraction (300 – 500 μm) was numerically
643 dominated by *Oithona similis* (50 % of the total mesozooplankton assemblage), although the
644 larger size fractions dominated the mesozooplankton biomass (dominated by *Clausocalanus*
645 *citer*, and *Rhicalanus gigas*). This is consistent with the dominance of small spherical faecal
646 pellets and the lower contribution of cylindrical shapes we observed in spring and early
647 summer (cups #1 to #4, October to December 2011, Table 6). In summer (January 2005), the
648 mesozooplankton community was more diversified and comprised 21 % of small individuals
649 (*Oithona* sp and *Oncea* sp.), 20 % of medium-sized individuals (*Clausocalanus* sp and
650 *Microcalanus* sp.) and 21 % of large individuals (*Calanus* sp., *Metridia* sp., *Paraeuchaeta* sp.,
651 *Pleuromama* sp. and *Rhincalanus* sp.; Carlotti et al., 2008). As the median size of faecal
652 pellets increases, so does their relative contribution to carbon flux (Fig. 5b and 5d, Table 6).
653 Our observation of an increasing contribution of cylindrical faecal pellet shapes in summer
654 (cups #5 to #10, December 2011 to February 2012, Table 6) is consistent with the increasing

655 contribution of large calanoid copepods to the mesozooplankton assemblages. We note that
656 pteropods showed the highest contribution to mesozooplankton assemblages at station A3 in
657 summer (16 % of total abundance, Carlotti et al., 2008). We associate this observation with
658 the large ellipsoid faecal pellet shape that was first observed in the sediment trap in cup #5
659 (end December 2011) and represented the highest contribution to faecal pellet carbon fluxes
660 in cup #9 (January/February 2012, Table 7). Tabular faecal pellets dominated the low POC
661 fluxes observed in the autumn and winter when chlorophyll *a* concentration was reduced to
662 background levels, although this interpretation should be taken with caution since a constant
663 and high carbon content was used for this shape. The increase in organic carbon content and
664 negative correlation between the abundance of cylindrical, ellipsoid and tabular faecal pellets
665 fluxes and the BSi:POC molar ratio suggests that large zooplankton producing these tabular
666 pellets (large copepods, euphausiids and salps) were not feeding directly on diatoms. During
667 the autumn and winter, microbial components other than diatoms must sustain the production
668 of these large zooplankton. Direct observation of faecal pellet content is beyond the scope of
669 the present study but would help to elucidate how seasonal trends of zooplankton feeding
670 ecology influence carbon and biomineral export. Moreover, dedicated studies are still needed
671 to document the seasonal dynamic of euphausiid and salp abundances over the Kerguelen
672 Plateau to compare them with our reported faecal pellet fluxes.

673 **4.3 Diatom fluxes**

674 The diatom fluxes (sum of empty and full cells) observed at the central Kerguelen
675 Plateau reached their maximum value of 1.2×10^8 cells $m^{-2} d^{-1}$ during the two short export
676 events, which is equivalent to 2.4×10^8 valves $m^{-2} d^{-1}$. This latter value falls between the
677 highest values observed in POOZ ($\sim 10^7$ valves $m^{-2} d^{-1}$ Abelmann and Gersonde, 1991; Salter
678 et al., 2012; Grigorov et al., 2014) and the SIZ ($> 10^9$ valves $m^{-2} d^{-1}$, Suzuki et al., 2001;
679 Pilskaln et al., 2004). The diatom fluxes over the Kerguelen plateau are similar to the 2.5 - 3.5

680 $\times 10^8$ valves $\text{m}^{-2} \text{ d}^{-1}$ measured at 200 m depth in a coastal station of the Antarctic Peninsula,
681 where CRS represented ~80 % of the phytoplankton assemblage (Leventer, 1991). Previous
682 studies report the presence of a resting spore formation strategy in diatom species as typically
683 associated with neritic areas (Smetacek, 1985; Crosta et al., 1997; Salter et al., 2012). During
684 the summer KEOPS1 cruise, a shift in plankton community composition was observed at
685 station A3 between January and February. The surface community initially dominated by
686 *Chaetoceros Hyalochaete* vegetative chains gave way to one dominated by *Eucampia*
687 *antarctica* var. *antarctica*, concomitant with increasing CRS abundance in the mixed layer
688 (Armand et al., 2008a). The abundance of dead cells (within chains or as empty single cells
689 and half cells) in the surface water column also increased from January to February,
690 suggesting intense heterotrophic activity. Surface sediments at station A3 contain, in
691 decreasing abundance, *F. kerguelensis*, CRS and *T. nitzschioides* spp. cells (Armand et al.,
692 2008b). These sedimentary distributions are consistent with the dominant species observed in
693 the sediment trap, *F. kerguelensis* and *T. nitzschioides* spp. being present throughout the year
694 and mostly represented by empty cells whereas CRS are exported during short and intense
695 events.

696 *Eucampia antarctica* var. *antarctica* resting spores dominated the deep (2000 m)
697 sediment trap diatom assemblages in the naturally fertilized area close to the Crozet Islands
698 with fluxes $> 10^7$ cells $\text{m}^{-2} \text{ d}^{-1}$ (Salter et al., 2012). We observed highest *Eucampia antarctica*
699 var. *antarctica* full cells fluxes of $\sim 10^6$ cells $\text{m}^{-2} \text{ d}^{-1}$ in summer, which represents < 10 % of the
700 total cell flux. Both vegetative and resting stages were observed. Our results suggest that
701 *Eucampia antarctica* var. *antarctica* is unlikely to be a major driving vector for carbon fluxes
702 to depth over the central Kerguelen Plateau, in part because the community was not forming
703 massive highly-silicified, fast-sinking resting spores contrary to observations near the Crozet
704 Islands. Moreover their biogeographic abundance distribution from sea floor observations

705 suggests they are not dominant in this region of the plateau (Armand et al., 2008b). The iron-
706 fertilized Crozet bloom is north of the Polar Front and dissolved Si(OH)₄ concentrations were
707 depleted to 0.2 $\mu\text{mol L}^{-1}$ (Salter et al., 2007) compared to \sim 2 $\mu\text{mol L}^{-1}$ on the Kerguelen
708 Plateau (Mosseri et al., 2008). It is possible, along with differences in iron dynamics between
709 the two plateaus, that differences in nutrient stoichiometry favour bloom dynamics and resting
710 spore formation of *Chaetoceros Hyalochaete* populations surrounding the Kerguelen Islands.
711 Nevertheless, the increasing full cell flux of *Eucampia antarctica* var. *antarctica* from spring
712 to summer in the sediment trap time series is consistent with the observations of an increasing
713 abundance in the mixed layer at the station A3 in summer (Armand et al., 2008a).

714 Highest *Pseudo-nitzschia* spp. full cell fluxes were observed in summer,
715 concomitantly with the second export peak (cup #9, end January 2012). *Pseudo-nitzschia*
716 species are rarely found in deep sediment trap studies and are absent from sediment diatom
717 assemblages, presumably due to their susceptibility to water column dissolution (Grigorov et
718 al., 2014; Rigual-Hernández et al., 2015). The species *Pseudo-nitzschia hemii* has been
719 reported to accumulate in summer in deep chlorophyll maximum in the Polar Frontal Zone
720 (Kopczynska et al., 2001). Such deep biomass accumulation is hypothesized to benefit from
721 nutrient diffusion through the pycnocline (Parslow et al., 2001). These general observations
722 are consistent with the peaks in *Pseudo-nitzschia* spp. fluxes we report in summer over the
723 Kerguelen Plateau.

724 Although their fluxes were very low, species of the *Rhizosolenia* and *Proboscia*
725 genera were mostly exported as empty cells at the end of summer and during autumn (cups #8
726 to #11, end January to May 2012), occurring in parallel with the full cell fluxes of the giant
727 diatom *Thalassiothrix antarctica* (Table 4). It has been suggested that these species belong to
728 a group of “deep shade flora” that accumulate at the subsurface chlorophyll maxima in
729 summer with their large frustules protecting them from grazing pressure in stratified waters

730 (Kemp and Villareal, 2013). Interestingly these species were also found in deep sediment
731 traps located in a HNLC area south of the Crozet Plateau (Salter et al., 2012), as well as in
732 subsurface chlorophyll maximum in HNLC waters of the Southern Ocean (Parslow et al.,
733 2001; Holm-Hansen et al., 2004; Gomi et al., 2010). A subsurface chlorophyll maximum has
734 previously been observed at 120 m on the Kerguelen Plateau (also station A3) during summer
735 (Uitz et al., 2009) and appears to correspond to an accumulation of particles consisting of
736 aggregates of large diatom species (Jouandet et al., 2011). The fact that *Rhizosolenia* spp. and
737 *Proboscia* spp. were observed as empty cells whereas *Thalassiothrix antarctica* was mostly
738 represented by full cells suggest species-specific grazing on these communities. There appears
739 to be ecological differentiation within the “deep shade flora” that precludes describing a
740 single effect on export stoichiometry. Moreover, on the Kerguelen Plateau, these species are
741 not exported in “massive” proportions as the fall-dump hypothesis suggests (Kemp et al.,
742 2000). The physical and biogeochemical factors responsible for their production and export
743 are still to be determined, and should be investigated thoroughly given the potential
744 importance that these species might have for export fluxes on a global scale (Kemp et al.,
745 2000; Richardson et al., 2000; Kemp and Villareal, 2013).

746 **4.4 Preferential carbon and silica sinkers**

747 Unlike most previous sediment trap studies in the Southern Ocean, we used a counting
748 technique that facilitated the identification of carbon and siliceous components of exported
749 material. Although we lost a small degree of taxonomic resolution with this approach (see
750 methods), it allowed us to avoid unnecessary assumptions concerning carbon content of
751 exported diatoms and directly constrain the role of different species for carbon and silica
752 export.

753 The annual BSi:POC ratio of the exported material (1.16) is much higher than the
754 usual ratio proposed for marine diatoms of 0.13 (Brzezinski, 1985). Moreover, the BSi:POC
755 ratio of the exported material in spring (2.1 to 3.4, cups #1 to #3, October to mid-December
756 2011) is significantly higher than the BSi:POC ratio of 0.32 ± 0.06 in the mixed layer of the
757 same station during spring (Lasbleiz et al., 2014). Numerous chemical, physical, biological
758 and ecological factors can impact BSi:POC ratios of marine diatoms (e.g. Ragueneau et al.,
759 2006). However, the ten-fold differences in BSi:POC ratios of exported particles between
760 spring and summer is unlikely to result only from physiological constraints set during diatoms
761 growth (Hutchins and Bruland, 1998; Takeda, 1998). Previous comparisons in natural and
762 artificially iron-fertilized settings have highlighted the importance of diatom community
763 structure for carbon and silica export (Smetacek et al., 2004; Salter et al., 2012; Quéguiner,
764 2013; Assmy et al., 2013). The presence of different diatom species and their characteristic
765 traits (e. g. susceptibility to grazing, apoptosis, viral lysis) are all likely to influence the flux
766 of full and empty cells. Therefore, the net BSi:POC export ratio results from the net effect of
767 species specific Si:C composition (Sackett et al., 2014) and the subsequent species-specific
768 mortality pathway and dissolution. A significant correlation between BSi:POC and empty:full
769 cells ratio (Spearman rank correlation, $n = 12$, $\rho = 0.78$, $p < 0.05$) suggests the latter acts as a
770 first order control on the silicon and organic carbon export stoichiometry. Differences in
771 BSi:POC ratios between the mixed layer suspended particle stock and particles exported out
772 of the mixed layer may be explained by the dominant sedimentation of empty diatom frustules
773 that results from the grazing pressure by the zooplankton community and the intense carbon
774 utilization by heterotrophic microbial communities (Christaki et al., 2014).

775 We classified species that were observed exclusively as empty cells, or sinking with an
776 integrated empty:full ratio >2 , as predominantly silica exporters and these included: *C. bulbosum*,
777 *C. pennatum*, *P. truncata*, *R. antennata/styliformis*, *A. hookeri*, *A. hyalinus*, *C.*

778 *decipiens*, *C. inerme*, *D. antarcticus*, *P. alata*, *T. nitzschioides* spp., *T. lentiginosa*, and small
779 centric species (< 20 μm). Although *F. kerguelensis*, *T. nitzschioides* spp. and *T. lentiginosa*
780 were present through the entire season, their fluxes were highly correlated with BSi:POC
781 ratios (Fig. 6) identifying these species as significant contributors to silica export. On the
782 contrary resting spores and species that sink with a major contribution of full cells (integrated
783 empty:full ratio <0.5) were identified as belonging to the preferential carbon sinkers: *C.*
784 *Hyalochaete* spp., *E. antarctica* var. *antarctica*, *R. simplex* and *Thalassiothrix antarctica*.
785 Among them, CRS and *E. antarctica* var. *antarctica* were the most negatively correlated to
786 the BSi:POC ratio and were identified as key species for carbon export (Fig. 6). These
787 observations are consistent with a previous study of natural iron fertilization that identified *C.*
788 *pennatum*, *D. antarcticus* and *F. kerguelensis* as major silica sinkers and CRS and *E.*
789 *antarctica* var. *antarctica* resting spores as major carbon sinkers downstream Crozet islands
790 (Salter et al., 2012). During the EIFEX artificial fertilization experiment *C. Hyalochaete*
791 vegetative stages were identified as major carbon sinker whereas *F. kerguelensis* was
792 considered as strong silica sinker (Assmy et al., 2013). Notably, resting spore formation was
793 not observed in the artificial experiment performed in the open ocean remote from coastal
794 influence, and carbon export was attributed to mass mortality and aggregation of algal cells
795 (Assmy et al., 2013). Nevertheless, a more detailed analysis of species-specific carbon and
796 silica content in the exported material is necessary to fully elucidate their respective roles on
797 carbon and silica export.

798 **4.5 Seasonal succession of ecological flux vectors over the Kerguelen Plateau**

799 Although sediment trap records integrate cumulative processes of production in the mixed
800 layer and selective losses during export, they provide a unique insight into the temporal
801 succession of plankton functional types and resultant geochemical properties of exported
802 particles characterizing the biological pump. The seasonal cycle of ecological vectors and

803 associated export stoichiometry is summarized in Figure 7. The robustness of the relationship
804 between measured and calculated POC fluxes (Fig. 8b) suggests that the main ecological flux
805 vectors described from the samples are capable of predicting seasonal patterns of total POC
806 fluxes. At an annual scale the calculated POC fluxes slightly underestimate the measured
807 fluxes (93.1 versus 98.2 mmol m⁻²). This might result from the minor contribution of full
808 cells other than the diatoms species considered, aggregated material, organic matter sorbed to
809 the exterior of empty cells and faecal fluff that was difficult to enumerate.

810 A scheme of phytoplankton and zooplankton communities succession in naturally-
811 fertilized areas of the Southern Ocean was proposed by Quéguiner (2013). Spring
812 phytoplankton communities are characterized by small, lightly silicified, fast growing diatoms
813 associated with small microphagous copepods. In summer, the phytoplankton community
814 progressively switches toward large, highly silicified, slow growing diatoms resistant to the
815 grazing by large copepods. In this scheme carbon export occurs mostly in end summer
816 through the fall dump. The species succession directly observed in our sediment trap samples
817 differs somewhat to the conceptual model proposed by Quéguiner (2013), although the
818 general patterns are similar. The diatom species exported in spring were *F. kerguelensis*, *T.*
819 *nitzschiooides* spp., and small centric species (<20 µm), whilst in summer the comparatively
820 very large (>200 µm) species of *Proboscia* sp., *Rhizosolenia* sp. and *Thalassiothrix antarctica*
821 were observed. However we observe that these species constituting the spring fluxes are
822 exported almost exclusively as empty cells. The abundance of small spherical and ovoid
823 faecal pellet suggests an important role of small copepods in the zooplankton (Yoon et al.,
824 2001; Wilson et al., 2013), which was corroborated by the finding of dominant *Oithona*
825 *similis* abundances in the spring mesozooplankton assemblages at station A3 (Carlotti et al.,
826 2015). Therefore, our data suggests that spring export captured by the sediment trap was the

827 remnants of a diatom community subject to efficient grazing and carbon utilization in, or at
828 the basis of, the mixed layer, resulting in a BSi:POC export ratio > 2 (Table 1).

829 The main difference in our observations and the conceptual scheme of Quéguiner,
830 (2013) is the dominance of *Chaetoceros Hyalochaete* resting spores to diatom export
831 assemblages and their contribution to carbon fluxes out of the mixed layer in summer. Resting
832 spores appear to efficiently bypass the “carbon trap” represented by grazers and might also
833 physically entrain small faecal pellets in their downward flux. In mid-summer, faecal pellet
834 carbon export is dominated by the contribution of cylindrical shapes. This appears to be
835 consistent with an observed shift toward a higher contribution of large copepods and
836 euphausiids to the mesozooplankton community in the mixed layer (Carlotti et al., 2008).
837 However, CRS still dominate the diatom exported assemblage. The corresponding BSi:POC
838 ratio decreases with values between 1 and 2 (Table 1). The fact that there are two discrete
839 resting spore export events might be explained by a mixing event that injected Si(OH)₄ into
840 the surface allowing the development of a secondary Si(OH)₄ limitation.

841 In the autumn and winter, diatom fluxes are very low and faecal pellet carbon export is
842 dominated by cylindrical and tabular contributions consistent with a supposed shift to
843 zooplankton communities dominated by large copepods, euphausiids, and salps (Wilson et al.,
844 2013). The low BSi:POC ratios characterizing export at this time suggest that these
845 communities feed primarily suspended particles (in the case of salps) and on micro- and
846 mesozooplankton or small diatoms, although direct measurements of faecal pellet content
847 would be necessary to confirm this.

848 **5 Conclusion**

849 We report the chemical (particulate organic carbon and nitrogen, biogenic silica) and
850 biological (diatom cells and faecal pellets) composition of material exported beneath the

851 winter mixed layer (289 m) in a naturally iron-fertilized area of the Southern Ocean. Annually
852 integrated organic carbon export from the iron-fertilized bloom was low (98 mmol m^{-2})
853 although biogenic silicon export was significant (114 mmol m^{-2}). *Chaetoceros Hyalochaete*
854 and *Thalassiosira antarctica* resting spores accounted for more than 60 % of the annual POC
855 flux. The high abundance of empty cells and the low contribution of faecal pellets to POC
856 flux (34 %) suggest efficient carbon retention occurs in, or at the base of the mixed layer. We
857 propose that in this HBLE environment, carbon-rich and fast-sinking resting spores bypass the
858 intense grazing pressure otherwise responsible for the rapid attenuation of flux. The seasonal
859 succession of diatom taxa groups was tightly linked to the stoichiometry of the exported
860 material. Several species were identified as primarily “silica sinkers” e.g. *Fragilariopsis*
861 *kerguelensis* and *Thalassionema nitzschiooides* spp. and others as preferential “carbon sinkers”
862 e.g. resting spores of *Chaetoceros Hyalochaete* and *Thalassiosira antarctica*, *Eucampia*
863 *antarctica* var. *antarctica* and the giant diatom *Thalassiothrix antarctica*. Faecal pellet types
864 described a clear transition from small spherical shapes (small copepods) in spring, larger
865 cylindrical an ellipsoid shapes in summer (euphausiids and large copepods) and large tabular
866 shape (salps) in fall. Their contribution to carbon fluxes increased with the presence of larger
867 shapes.

868 The change in biological productivity and ocean circulation cannot explain the ~80
869 ppmv atmospheric pCO_2 difference between the preindustrial era and the last glacial
870 maximum (Archer et al., 2000; Bopp et al., 2003; Kohfeld et al., 2005; Wolff et al., 2006).
871 Nevertheless, a simple switch in ‘silica sinker’ versus ‘carbon sinker’ relative abundance
872 would have a drastic effect on carbon sequestration in the Southern Ocean and silicic acid
873 availability at lower latitudes (Sarmiento et al., 2004; Boyd, 2013). The results presented here
874 emphasize the compelling need for similar studies in other locations of the global Ocean that

875 will allow identification of key ecological vectors that set the magnitude and the
876 stoichiometry of the biological pump.

877 **Acknowledgements**

878 We thank the Captain Bernard Lassiette and his crew during the KEOPS2 mission on the R/V
879 *Marion Dufresne II*. We thank Karine Leblanc and Marine Lasbleiz and three anonymous
880 reviewers for their constructive comments, which helped us to improve the manuscript. This
881 work was supported by the French Research program of INSU-CNRS LEFE-CYBER (Les
882 enveloppes fluides et l'environnement – Cycles biogéochimiques, environnement et
883 ressources), the French ANR (Agence Nationale de la Recherche, SIMI-6 program, ANR-10-
884 BLAN-0614), the French CNES (Centre National d'Etudes Spatiales) and the French Polar
885 Institute IPEV (Institut Polaire Paul-Emile Victor). L. Armand's participation in the KEOPS2
886 program was supported by an Australian Antarctic Division grant (#3214).

888 Abdi, H., 2010. Partial least squares regression and projection on latent structure regression (PLS
889 Regression). *Wiley Interdiscip. Rev. Comput. Stat.* 2, 97–106. doi:10.1002/wics.51

890 Abelmann, A., Gersonde, R., 1991. Biosiliceous particle flux in the Southern Ocean. *Mar. Chem.*,
891 Biochemistry and circulation of water masses in the Southern Ocean International Symposium
892 35, 503–536. doi:10.1016/S0304-4203(09)90040-8

893 Allen, C.S., Pike, J., Pudsey, C.J., Leventer, A., 2005. Submillennial variations in ocean conditions
894 during deglaciation based on diatom assemblages from the southwest Atlantic.
895 *Paleoceanography* 20, PA2012. doi:10.1029/2004PA001055

896 Aminot, A., Kerouel, R., 2007. Dosage automatique des nutriments dans les eaux marines: méthodes
897 en flux continu. Ifremer, Plouzané, France.

898 Archer, D., Winguth, A., Lea, D., Mahowald, N., 2000. What caused the glacial/interglacial
899 atmospheric pCO₂ cycles? *Rev. Geophys.* 38, 159–189. doi:10.1029/1999RG000066

900 Armand, L.K., Cornet-Barthaux, V., Mosseri, J., Quéguiner, B., 2008a. Late summer diatom biomass
901 and community structure on and around the naturally iron-fertilised Kerguelen Plateau in the
902 Southern Ocean. *Deep Sea Res. Part II Top. Stud. Oceanogr.*, KEOPS: Kerguelen Ocean and
903 Plateau compared Study 55, 653–676. doi:10.1016/j.dsr2.2007.12.031

904 Armand, L.K., Crosta, X., Quéguiner, B., Mosseri, J., Garcia, N., 2008b. Diatoms preserved in surface
905 sediments of the northeastern Kerguelen Plateau. *Deep Sea Res. Part II Top. Stud. Oceanogr.*
906 55, 677–692. doi:10.1016/j.dsr2.2007.12.032

907 Armand, L.K., Crosta, X., Romero, O., Pichon, J.-J., 2005. The biogeography of major diatom taxa in
908 Southern Ocean sediments: 1. Sea ice related species. *Palaeogeogr. Palaeoclimatol.*
909 *Palaeoecol.* 223, 93–126. doi:10.1016/j.palaeo.2005.02.015

910 Arrigo, K.R., Worthen, D., Schnell, A., Lizotte, M.P., 1998. Primary production in Southern Ocean
911 waters. *J. Geophys. Res. Oceans* 103, 15587–15600. doi:10.1029/98JC00930

912 Assmy, P., Smetacek, V., Montresor, M., Klaas, C., Henjes, J., Strass, V.H., Arrieta, J.M., Bathmann,
913 U., Berg, G.M., Breitbarth, E., Cisewski, B., Friedrichs, L., Fuchs, N., Herndl, G.J., Jansen, S.,
914 Krägesky, S., Latasa, M., Peeken, I., Röttgers, R., Scharek, R., Schüller, S.E., Steigenberger,
915 S., Webb, A., Wolf-Gladrow, D., 2013. Thick-shelled, grazer-protected diatoms decouple
916 ocean carbon and silicon cycles in the iron-limited Antarctic Circumpolar Current. *Proc. Natl.*
917 *Acad. Sci.* 110, 20633–20638. doi:10.1073/pnas.1309345110

918 Baker, E.T., Milburn, H.B., Tennant, D.A., 1988. Field assessment of sediment trap efficiency under
919 varying flow conditions. *J. Mar. Res.* 46, 573–592. doi:10.1357/002224088785113522

920 Bao, R., Stigter, H.D., Weering, T.C.E.V., 2000. Diatom fluxes in surface sediments of the Goban
921 Spur continental margin, NE Atlantic Ocean. *J. Micropalaeontology* 19, 123–131.
922 doi:10.1144/jm.19.2.123

923 Blain, S., Quéguiner, B., Armand, L., Belviso, S., Bomblet, B., Bopp, L., Bowie, A., Brunet, C.,
924 Brussaard, C., Carlotti, F., Christaki, U., Corbière, A., Durand, I., Ebersbach, F., Fuda, J.-L.,
925 Garcia, N., Gerringa, L., Griffiths, B., Guigue, C., Guillerm, C., Jacquet, S., Jeandel, C., Laan,
926 P., Lefèvre, D., Lo Monaco, C., Malits, A., Mosseri, J., Obernosterer, I., Park, Y.-H., Picheral,
927 M., Pondaven, P., Remenyi, T., Sandroni, V., Sarthou, G., Savoye, N., Scouarnec, L.,
928 Souhaut, M., Thuiller, D., Timmermans, K., Trull, T., Uitz, J., van Beek, P., Veldhuis, M.,
929 Vincent, D., Viollier, E., Vong, L., Wagener, T., 2007. Effect of natural iron fertilization on
930 carbon sequestration in the Southern Ocean. *Nature* 446, 1070–1074.
931 doi:10.1038/nature05700

932 Blain, S., Renaut, S., Xing, X., Claustre, H., Guinet, C., 2013. Instrumented elephant seals reveal the
933 seasonality in chlorophyll and light-mixing regime in the iron-fertilized Southern Ocean.
934 *Geophys. Res. Lett.* 40, 6368–6372. doi:10.1002/2013GL058065

935 Blain, S., Tréguer, P., Belviso, S., Bucciarelli, E., Denis, M., Desabre, S., Fiala, M., Martin Jézéquel,
936 V., Le Fèvre, J., Mayzaud, P., Marty, J.-C., Razouls, S., 2001. A biogeochemical study of the
937 island mass effect in the context of the iron hypothesis: Kerguelen Islands, Southern Ocean.
938 *Deep Sea Res. Part Oceanogr. Res. Pap.* 48, 163–187. doi:10.1016/S0967-0637(00)00047-9

939 Bodungen, B. von, 1986. Phytoplankton growth and krill grazing during spring in the Bransfield
940 Strait, Antarctica — Implications from sediment trap collections. *Polar Biol.* 6, 153–160.
941 doi:10.1007/BF00274878

942 Bopp, L., Kohfeld, K.E., Le Quéré, C., Aumont, O., 2003. Dust impact on marine biota and
943 atmospheric CO₂ during glacial periods. *Paleoceanography* 18, 1046.
944 doi:10.1029/2002PA000810

945 Bowie, A.R., van der Merwe, P., Quérouté, F., Trull, T., Fourquez, M., Planchon, F., Sarthou, G.,
946 Chever, F., Townsend, A.T., Obernosterer, I., Sallée, J.-B., Blain, S., 2014. Iron budgets for
947 three distinct biogeochemical sites around the Kerguelen archipelago (Southern Ocean) during
948 the natural fertilisation experiment KEOPS-2. *Biogeosciences Discuss* 11, 17861–17923.
949 doi:10.5194/bgd-11-17861-2014

950 Boyd, P.W., 2013. Diatom traits regulate Southern Ocean silica leakage. *Proc. Natl. Acad. Sci.* 110,
951 20358–20359. doi:10.1073/pnas.1320327110

952 Brzezinski, M.A., 1985. The Si:C:N ratio of marine diatoms: interspecific variability and the effect of
953 some environmental variables. *J. Phycol.* 21, 347–357. doi:10.1111/j.0022-3646.1985.00347.x

954 Brzezinski, M.A., Pride, C.J., Franck, V.M., Sigman, D.M., Sarmiento, J.L., Matsumoto, K., Gruber,
955 N., Rau, G.H., Coale, K.H., 2002. A switch from Si(OH)4 to NO₃[–] depletion in the glacial
956 Southern Ocean. *Geophys. Res. Lett.* 29. doi:10.1029/2001GL014349

957 Buesseler, K.O., 1998. The decoupling of production and particulate export in the surface ocean. *Glob.*
958 *Biogeochem. Cycles* 12, 297–310. doi:10.1029/97GB03366

959 Buesseler, K.O., Antia, A.N., Chen, M., Fowler, S.W., Gardner, W.D., Gustafsson, Ö., Harada, K.,
960 Michaels, A.F., Rutgers v. d. Loeff, M., Sarin, M., Steinberg, D.K., Trull, T., 2007. An
961 assessment of the use of sediment traps for estimating upper ocean particle fluxes. *J. Mar. Res.*
962 65, 345–416.

963 Buesseler, K.O., Steinberg, D.K., Michaels, A.F., Johnson, R.J., Andrews, J.E., Valdes, J.R., Price,
964 J.F., 2000. A comparison of the quantity and composition of material caught in a neutrally
965 buoyant versus surface-tethered sediment trap. *Deep Sea Res. Part Oceanogr. Res. Pap.* 47,
966 277–294. doi:10.1016/S0967-0637(99)00056-4

967 Burd, A.B., Jackson, G.A., 2009. Particle Aggregation. *Annu. Rev. Mar. Sci.* 1, 65–90.
968 doi:10.1146/annurev.marine.010908.163904

969 Carlotti, F., Jouandet, M.-P., Nowaczyk, A., Harmelin-Vivien, M., Lefèvre, D., Guillou, G., Zhu, Y.,
970 Zhou, M., 2015. Mesozooplankton structure and functioning during the onset of the Kerguelen
971 phytoplankton bloom during the Keops2 survey. *Biogeosciences Discuss* 12, 2381–2427.
972 doi:10.5194/bgd-12-2381-2015

973 Carlotti, F., Thibault-Botha, D., Nowaczyk, A., Lefèvre, D., 2008. Zooplankton community structure,
974 biomass and role in carbon fluxes during the second half of a phytoplankton bloom in the
975 eastern sector of the Kerguelen Shelf (January–February 2005). *Deep Sea Res. Part II Top.*
976 *Stud. Oceanogr.*, KEOPS: Kerguelen Ocean and Plateau compared Study 55, 720–733.
977 doi:10.1016/j.dsr2.2007.12.010

978 Cavan, E.L., Le Moigne, F. A. C., Poulton, A.J., Tarling, G.A., Ward, P., Daniels, C.J., Fragoso, G.,
979 Sanders, R.J., 2015. Zooplankton fecal pellets control the attenuation of particulate organic
980 carbon flux in the Scotia Sea, Southern Ocean. *Geophys. Res. Lett.* 2014GL062744.
981 doi:10.1002/2014GL062744

982 Chang, A.S., Bertram, M.A., Ivanochko, T., Calvert, S.E., Dallimore, A., Thomson, R.E., 2013.
983 Annual record of particle fluxes, geochemistry and diatoms in Effingham Inlet, British
984 Columbia, Canada, and the impact of the 1999 La Niña event. *Mar. Geol.* 337, 20–34.
985 doi:10.1016/j.margeo.2013.01.003

986 Christaki, U., Lefèvre, D., Georges, C., Colombet, J., Catala, P., Courties, C., Sime-Ngando, T., Blain,
987 S., Obernosterer, I., 2014. Microbial food web dynamics during spring phytoplankton blooms
988 in the naturally iron-fertilized Kerguelen area (Southern Ocean). *Biogeosciences* 11, 6739–
989 6753. doi:10.5194/bgd-11-6739-2014

990 Closset, I., Lasbleiz, M., Leblanc, K., Quéguiner, B., Cavagna, A.-J., Elskens, M., Navez, J., Cardinal,
991 D., 2014. Seasonal evolution of net and regenerated silica production around a natural Fe-
992 fertilized area in the Southern Ocean estimated with Si isotopic approaches. *Biogeosciences*
993 11, 5827–5846. doi:10.5194/bgd-11-5827-2014

994 Cornet-Barthaux, V., Armand, L., Quguiner, B., 2007. Biovolume and biomass estimates of key
995 diatoms in the Southern Ocean. *Aquat. Microb. Ecol.* 48, 295–308. doi:10.3354/ame048295

996 Crawford, R., 1995. The role of sex in the sedimentation of a marine diatom bloom. *Limnol.*
997 *Oceanogr.* 40, 200–204.

998 Crosta, X., Pichon, J.-J., Labracherie, M., 1997. Distribution of *Chaetoceros* resting spores in modern
999 peri-Antarctic sediments. *Mar. Micropaleontol.* 29, 283–299. doi:10.1016/S0377-
1000 8398(96)00033-3

1001 Davison, P.C., Checkley Jr., D.M., Koslow, J.A., Barlow, J., 2013. Carbon export mediated by
1002 mesopelagic fishes in the northeast Pacific Ocean. *Prog. Oceanogr.* 116, 14–30.
1003 doi:10.1016/j.pocean.2013.05.013

1004 DeMaster, D.J., 1981. The supply and accumulation of silica in the marine environment. *Geochim.
1005 Cosmochim. Acta* 45, 1715–1732. doi:10.1016/0016-7037(81)90006-5

1006 Doucette, G.J., Fryxell, G.A., 1983. *Thalassiosira antarctica*: vegetative and resting stage chemical
1007 composition of an ice-related marine diatom. *Mar. Biol.* 78, 1–6. doi:10.1007/BF00392964

1008 Dubischar, C.D., Bathmann, U.V., 2002. The occurrence of faecal material in relation to different
1009 pelagic systems in the Southern Ocean and its importance for vertical flux. *Deep Sea Res. Part
1010 II Top. Stud. Oceanogr., The Southern Ocean II: Climatic Changes and the Cycle of Carbon*
1011 49, 3229–3242. doi:10.1016/S0967-0645(02)00080-2

1012 Dunbar, R.B., 1984. Sediment trap experiments on the Antarctic continental margin. *Antarct. J. US*
1013 70–71.

1014 Dutkiewicz, S., Follows, M.J., Parekh, P., 2005. Interactions of the iron and phosphorus cycles: A
1015 three-dimensional model study. *Glob. Biogeochem. Cycles* 19, GB1021.
1016 doi:10.1029/2004GB002342

1017 Ebersbach, F., Assmy, P., Martin, P., Schulz, I., Wolzenburg, S., Nöthig, E.-M., 2014. Particle flux
1018 characterisation and sedimentation patterns of protistan plankton during the iron fertilisation
1019 experiment LOHAFEX in the Southern Ocean. *Deep Sea Res. Part Oceanogr. Res. Pap.* 89,
1020 94–103. doi:10.1016/j.dsr.2014.04.007

1021 Ebersbach, F., Trull, T.W., 2008. Sinking particle properties from polyacrylamide gels during the
1022 Kerguelen Ocean and Plateau compared Study (KEOPS): Zooplankton control of carbon
1023 export in an area of persistent natural iron inputs in the Southern Ocean. *Limnol. Oceanogr.*
1024 53, 212–224. doi:10.4319/lo.2008.53.1.0212

1025 Ebersbach, F., Trull, T.W., Davies, D.M., Bray, S.G., 2011. Controls on mesopelagic particle fluxes in
1026 the Sub-Antarctic and Polar Frontal Zones in the Southern Ocean south of Australia in
1027 summer—Perspectives from free-drifting sediment traps. *Deep Sea Res. Part II Top. Stud.
1028 Oceanogr.* 58, 2260–2276. doi:10.1016/j.dsr2.2011.05.025

1029 Fischer, G., Fütterer, D., Gersonde, R., Honjo, S., Ostermann, D., Wefer, G., 1988. Seasonal
1030 variability of particle flux in the Weddell Sea and its relation to ice cover. *Nature* 335, 426–
1031 428. doi:10.1038/335426a0

1032 Fischer, G., Gersonde, R., Wefer, G., 2002. Organic carbon, biogenic silica and diatom fluxes in the
1033 marginal winter sea-ice zone and in the Polar Front Region: interannual variations and
1034 differences in composition. *Deep Sea Res. Part II Top. Stud. Oceanogr.* 49, 1721–1745.
1035 doi:10.1016/S0967-0645(02)00009-7

1036 Fransz, H.G., Gonzalez, S.R., 1995. The production of *Oithona similis* (Copepoda: Cyclopoida) in the
1037 Southern Ocean. *ICES J. Mar. Sci. J. Cons.* 52, 549–555. doi:10.1016/1054-3139(95)80069-7

1038 Garrison, D.L., 1981. Monterey Bay Phytoplankton. II. Resting Spore Cycles in Coastal Diatom
1039 Populations. *J. Plankton Res.* 3, 137–156. doi:10.1093/plankt/3.1.137

1040 Gersonde, R., Zielinski, U., 2000. The reconstruction of late Quaternary Antarctic sea-ice
1041 distribution—the use of diatoms as a proxy for sea-ice. *Palaeogeogr. Palaeoclimatol.
1042 Palaeoecol.* 162, 263–286. doi:10.1016/S0031-0182(00)00131-0

1043 Gleiber, M.R., Steinberg, D.K., Ducklow, H.W., 2012. Time series of vertical flux of zooplankton
1044 fecal pellets on the continental shelf of the western Antarctic Peninsula. *Mar. Ecol. Prog. Ser.*
1045 471, 23–36. doi:10.3354/meps10021

1046 Gomi, Y., Fukuchi, M., Taniguchi, A., 2010. Diatom assemblages at subsurface chlorophyll maximum
1047 layer in the eastern Indian sector of the Southern Ocean in summer. *J. Plankton Res.* 32, 1039–
1048 1050. doi:10.1093/plankt/fbq031

1049 Gonzalez, H.E., Smetacek, V., 1994. The possible role of the cyclopoid copepod *Oithona* in retarding
1050 vertical flux of zooplankton faecal material. *Mar. Ecol.-Prog. Ser.* 113, 233–246.

1051 Grigorov, I., Rigual-Hernandez, A.S., Honjo, S., Kemp, A.E.S., Armand, L.K., 2014. Settling fluxes
1052 of diatoms to the interior of the Antarctic circumpolar current along 170 °W. *Deep Sea Res. Part Oceanogr. Res. Pap.* 93, 1–13. doi:10.1016/j.dsr.2014.07.008

1053 Grimm, K.A., Lange, C.B., Gill, A.S., 1996. Biological forcing of hemipelagic sedimentary laminae; evidence from ODP Site 893, Santa Barbara Basin, California. *J. Sediment. Res.* 66, 613–624. doi:10.1306/D42683C4-2B26-11D7-8648000102C1865D

1054 Hasle, G.R., Syvertsen, E.E., 1997. Chapter 2 - Marine Diatoms, in: Tomas, C.R. (Ed.), *Identifying Marine Phytoplankton*. Academic Press, San Diego, pp. 5–385.

1055 Hillebrand, H., Dürselen, C.-D., Kirschtel, D., Pollingher, U., Zohary, T., 1999. Biovolume Calculation for Pelagic and Benthic Microalgae. *J. Phycol.* 35, 403–424. doi:10.1046/j.1529-8817.1999.3520403.x

1056 Holm-Hansen, O., Kahru, M., Hewes, C.D., Kawaguchi, S., Kameda, T., Sushin, V.A., Krasovski, I., Priddle, J., Korb, R., Hewitt, R.P., Mitchell, B.G., 2004. Temporal and spatial distribution of chlorophyll-a in surface waters of the Scotia Sea as determined by both shipboard measurements and satellite data. *Deep Sea Res. Part II Top. Stud. Oceanogr.* 51, 1323–1331. doi:10.1016/j.dsr2.2004.06.004

1057 Holzer, M., Primeau, F.W., DeVries, T., Matear, R., 2014. The Southern Ocean silicon trap: Data-constrained estimates of regenerated silicic acid, trapping efficiencies, and global transport paths. *J. Geophys. Res. Oceans* 119, 313–331. doi:10.1002/2013JC009356

1058 Howard, A.G., Coxhead, A.J., Potter, I.A., Watt, A.P., 1986. Determination of dissolved aluminium by the micelle-enhanced fluorescence of its lumogallion complex. *Analyst* 111, 1379–1382. doi:10.1039/AN9861101379

1059 Hutchins, D.A., Bruland, K.W., 1998. Iron-limited diatom growth and Si:N uptake ratios in a coastal upwelling regime. *Nature* 393, 561–564. doi:10.1038/31203

1060 Ichinomiya, M., Gomi, Y., Nakamachi, M., Honda, M., Fukuchi, M., Taniguchi, A., 2008. Temporal variations in the abundance and sinking flux of diatoms under fast ice in summer near Syowa Station, East Antarctica. *Polar Sci.* 2, 33–40. doi:10.1016/j.polar.2008.01.001

1061 Jackson, G.A., Burd, A.B., 2001. A model for the distribution of particle flux in the mid-water column controlled by subsurface biotic interactions. *Deep Sea Res. Part II Top. Stud. Oceanogr., The US JGOFS Synthesis and Modeling Project: Phase 1* 49, 193–217. doi:10.1016/S0967-0645(01)00100-X

1062 Jackson, G.A., Waite, A.M., Boyd, P.W., 2005. Role of algal aggregation in vertical carbon export during SOIREE and in other low biomass environments. *Geophys. Res. Lett.* 32, L13607. doi:10.1029/2005GL023180

1063 Jin, X., Gruber, N., Dunne, J.P., Sarmiento, J.L., Armstrong, R.A., 2006. Diagnosing the contribution of phytoplankton functional groups to the production and export of particulate organic carbon, CaCO₃, and opal from global nutrient and alkalinity distributions. *Glob. Biogeochem. Cycles* 20, GB2015. doi:10.1029/2005GB002532

1064 Jouandet, M.-P., Blain, S., Metzl, N., Brunet, C., Trull, T.W., Obernosterer, I., 2008. A seasonal carbon budget for a naturally iron-fertilized bloom over the Kerguelen Plateau in the Southern Ocean. *Deep Sea Res. Part II Top. Stud. Oceanogr., KEOPS: Kerguelen Ocean and Plateau compared Study* 55, 856–867. doi:10.1016/j.dsr2.2007.12.037

1065 Jouandet, M.-P., Jackson, G.A., Carlotti, F., Picheral, M., Stemmann, L., Blain, S., 2014. Rapid formation of large aggregates during the spring bloom of Kerguelen Island: observations and model comparisons. *Biogeosciences* 11, 4393–4406. doi:10.5194/bg-11-4393-2014

1066 Jouandet, M.-P., Trull, T.W., Guidi, L., Picheral, M., Ebersbach, F., Stemmann, L., Blain, S., 2011. Optical imaging of mesopelagic particles indicates deep carbon flux beneath a natural iron-fertilized bloom in the Southern Ocean. *Limnol. Oceanogr.* 56, 1130–1140. doi:10.4319/lo.2011.56.3.1130

1067 Kato, M., Tanimura, Y., Matsuoka, K., Fukusawa, H., 2003. Planktonic diatoms from sediment traps in Omura Bay, western Japan with implications for ecological and taphonomic studies of coastal marine environments. *Quat. Int.* 105, 25–31. doi:10.1016/S1040-6182(02)00147-7

1103 Kemp, A.E.S., Pike, J., Pearce, R.B., Lange, C.B., 2000. The “Fall dump” — a new perspective on the
1104 role of a “shade flora” in the annual cycle of diatom production and export flux. Deep Sea
1105 Res. Part II Top. Stud. Oceanogr. 47, 2129–2154. doi:10.1016/S0967-0645(00)00019-9

1106 Kemp, A.E.S., Villareal, T.A., 2013. High diatom production and export in stratified waters – A
1107 potential negative feedback to global warming. Prog. Oceanogr. 119, 4–23.
1108 doi:10.1016/j.pocean.2013.06.004

1109 Kohfeld, K.E., Quéré, C.L., Harrison, S.P., Anderson, R.F., 2005. Role of Marine Biology in Glacial-
1110 Interglacial CO₂ Cycles. Science 308, 74–78. doi:10.1126/science.1105375

1111 Kopczynska, E.E., Dehairs, F., Elskens, M., Wright, S., 2001. Phytoplankton and microzooplankton
1112 variability between the Subtropical and Polar Fronts south of Australia: Thriving under
1113 regenerative and new production in late summer. J. Geophys. Res. Oceans 106, 31597–31609.
1114 doi:10.1029/2000JC000278

1115 Kuwata, A., Hama, T., Takahashi, M., 1993. Ecophysiological characterization of two life forms,
1116 resting spores and resting cells, of a marine planktonic diatom. Mar. Ecol. Prog. Ser. 102,
1117 245–255.

1118 Kuwata, A., Tsuda, A., 2005. Selection and viability after ingestion of vegetative cells, resting spores
1119 and resting cells of the marine diatom, *Chaetoceros pseudocurvatus*, by two copepods. J. Exp. Mar. Biol. Ecol. 322, 143–151. doi:10.1016/j.jembe.2005.02.013

1120 Lampitt, R.S., Boorman, B., Brown, L., Lucas, M., Salter, I., Sanders, R., Saw, K., Seeyave, S.,
1121 Thomalla, S.J., Turnewitsch, R., 2008. Particle export from the euphotic zone: Estimates using
1122 a novel drifting sediment trap, 234Th and new production. Deep Sea Res. Part Oceanogr. Res.
1123 Pap. 55, 1484–1502. doi:10.1016/j.dsr.2008.07.002

1124 Lampitt, R.S., Noji, T., Bodungen, B. von, 1990. What happens to zooplankton faecal pellets?
1125 Implications for material flux. Mar. Biol. 104, 15–23. doi:10.1007/BF01313152

1126 Lampitt, R.S., Salter, I., Johns, D., 2009. Radiolaria: Major exporters of organic carbon to the deep
1127 ocean. Glob. Biogeochem. Cycles 23, GB1010. doi:10.1029/2008GB003221

1128 Lam, P.J., Bishop, J.K.B., 2007. High biomass, low export regimes in the Southern Ocean. Deep Sea
1129 Res. Part II Top. Stud. Oceanogr. 54, 601–638. doi:10.1016/j.dsr2.2007.01.013

1130 Lam, P.J., Doney, S.C., Bishop, J.K.B., 2011. The dynamic ocean biological pump: Insights from a
1131 global compilation of particulate organic carbon, CaCO₃, and opal concentration profiles from
1132 the mesopelagic. Glob. Biogeochem. Cycles 25, GB3009. doi:10.1029/2010GB003868

1133 Lange, 1997. Sedimentation patterns of diatoms, radiolarians, and silicoflagellates in Santa Barbara
1134 Basin, California. Calif. Coop. Ocean. Fish. Investig. Rep. 38, 161–170.

1135 Lange, C.B., Weinheimer, A.L., Reid, F.M.H., Thunell, R.C., 1997. Sedimentation patterns of
1136 diatoms, radiolarians, and silicoflagellates in Santa Barbara Basin, California. Calif. Coop.
1137 Ocean. Fish. Investig. Rep. 38, 161–170.

1138 Lasbleiz, M., Leblanc, K., Blain, S., Ras, J., Cornet-Barthaux, V., Hélias Nunige, S., Quéguiner, B.,
1139 2014. Pigments, elemental composition (C, N, P, and Si), and stoichiometry of particulate
1140 matter in the naturally iron fertilized region of Kerguelen in the Southern Ocean.
1141 Biogeosciences 11, 5931–5955. doi:10.5194/bg-11-5931-2014

1142 Laurenceau, E.C., Trull, T.W., Davies, D.M., Bray, S.G., Doran, J., Planchon, F., Carlotti, F.,
1143 Jouandet, M.-P., Cavagna, A.-J., Waite, A.M., Blain, S., 2014. The relative importance of
1144 phytoplankton aggregates and zooplankton fecal pellets to carbon export: insights from free-
1145 drifting sediment trap deployments in naturally iron-fertilised waters near the Kerguelen
1146 plateau. Biogeosciences Discuss 11, 13623–13673. doi:10.5194/bgd-11-13623-2014

1147 Legendre, P., Dr, L.F.J.L., 1998. Numerical Ecology, Édition : 2. ed. Elsevier Science, Amsterdam ;
1148 New York.

1149 Leventer, A., 1991. Sediment trap diatom assemblages from the northern Antarctic Peninsula region.
1150 Deep Sea Res. Part Oceanogr. Res. Pap. 38, 1127–1143. doi:10.1016/0198-0149(91)90099-2

1151 Leventer, A., Dunbar, R.B., 1987. Diatom flux in McMurdo Sound, Antarctica. Mar. Micropaleontol.
1152 12, 49–64. doi:10.1016/0377-8398(87)90013-2

1153 Lopes, C., Mix, A.C., Abrantes, F., 2006. Diatoms in northeast Pacific surface sediments as
1154 paleoceanographic proxies. Mar. Micropaleontol. 60, 45–65.
1155 doi:10.1016/j.marmicro.2006.02.010

1156

1157 Madin, L.P., 1982. Production, composition and sedimentation of salp fecal pellets in oceanic waters.
1158 *Mar. Biol.* 67, 39–45. doi:10.1007/BF00397092

1159 Maiti, K., Charette, M.A., Buesseler, K.O., Kahru, M., 2013. An inverse relationship between
1160 production and export efficiency in the Southern Ocean. *Geophys. Res. Lett.* 40, 1557–1561.
1161 doi:10.1002/grl.50219

1162 Martin, J.H., Gordon, R.M., Fitzwater, S.E., 1990. Iron in Antarctic waters. *Nature* 345, 156–158.
1163 doi:10.1038/345156a0

1164 Matsumoto, K., Sarmiento, J.L., Brzezinski, M.A., 2002. Silicic acid leakage from the Southern
1165 Ocean: A possible explanation for glacial atmospheric pCO₂. *Glob. Biogeochem. Cycles* 16,
1166 5–1. doi:10.1029/2001GB001442

1167 McQuoid, M.R., Hobson, L.A., 1996. Diatom Resting Stages. *J. Phycol.* 32, 889–902.
1168 doi:10.1111/j.0022-3646.1996.00889.x

1169 Menden-Deuer, S., Lessard, E.J., 2000. Carbon to volume relationships for dinoflagellates, diatoms,
1170 and other protist plankton. *Limnol. Oceanogr.* 45, 569–579. doi:10.4319/lo.2000.45.3.0569

1171 Moore, C.M., Mills, M.M., Arrigo, K.R., Berman-Frank, I., Bopp, L., Boyd, P.W., Galbraith, E.D.,
1172 Geider, R.J., Guieu, C., Jaccard, S.L., Jickells, T.D., La Roche, J., Lenton, T.M., Mahowald,
1173 N.M., Marañón, E., Marinov, I., Moore, J.K., Nakatsuka, T., Oschlies, A., Saito, M.A.,
1174 Thingstad, T.F., Tsuda, A., Ulloa, O., 2013. Processes and patterns of oceanic nutrient
1175 limitation. *Nat. Geosci.* 6, 701–710. doi:10.1038/ngeo1765

1176 Moore, J.K., Doney, S.C., Glover, D.M., Fung, I.Y., 2001. Iron cycling and nutrient-limitation patterns
1177 in surface waters of the World Ocean. *Deep Sea Res.* 49, 463–507. doi:10.1016/S0967-
1178 0645(01)00109-6

1179 Mortlock, R.A., Froelich, P.N., 1989. A simple method for the rapid determination of biogenic opal in
1180 pelagic marine sediments. *Deep Sea Res. Part Oceanogr. Res. Pap.* 36, 1415–1426.
1181 doi:10.1016/0198-0149(89)90092-7

1182 Mosseri, J., Quéguiner, B., Armand, L., Cornet-Barthaux, V., 2008. Impact of iron on silicon
1183 utilization by diatoms in the Southern Ocean: A case study of Si/N cycle decoupling in a
1184 naturally iron-enriched area. *Deep Sea Res. Part II Top. Stud. Oceanogr.*, KEOPS: Kerguelen
1185 Ocean and Plateau compared Study 55, 801–819. doi:10.1016/j.dsr2.2007.12.003

1186 Nelson, D.M., Brzezinski, M.A., Sigmon, D.E., Franck, V.M., 2001. A seasonal progression of Si
1187 limitation in the Pacific sector of the Southern Ocean. *Deep Sea Res. Part II Top. Stud.*
1188 *Oceanogr.* 48, 3973–3995. doi:10.1016/S0967-0645(01)00076-5

1189 Nelson, D.M., Tréguer, P., Brzezinski, M.A., Leynaert, A., Quéguiner, B., 1995. Production and
1190 dissolution of biogenic silica in the ocean: Revised global estimates, comparison with regional
1191 data and relationship to biogenic sedimentation. *Glob. Biogeochem. Cycles* 9, 359–372.
1192 doi:10.1029/95GB01070

1193 Obernosterer, I., Christaki, U., Lefèvre, D., Catala, P., Van Wambeke, F., Lebaron, P., 2008. Rapid
1194 bacterial mineralization of organic carbon produced during a phytoplankton bloom induced by
1195 natural iron fertilization in the Southern Ocean. *Deep Sea Res. Part II Top. Stud. Oceanogr.*
1196 55, 777–789. doi:10.1016/j.dsr2.2007.12.005

1197 Oku, O., Kamatani, A., 1997. Resting spore formation of the marine planktonic diatom *Chaetoceros*
1198 *anastomosans* induced by high salinity and nitrogen depletion. *Mar. Biol.* 127, 515–520.
1199 doi:10.1007/s002270050040

1200 Onodera, J., Watanabe, E., Harada, N., Honda, M.C., 2014. Diatom flux reflects water-mass
1201 conditions on the southern Northwind Abyssal Plain, Arctic Ocean. *Biogeosciences Discuss*
1202 11, 15215–15250. doi:10.5194/bgd-11-15215-2014

1203 Park, J., Oh, I.-S., Kim, H.-C., Yoo, S., 2010. Variability of SeaWiFs chlorophyll-a in the southwest
1204 Atlantic sector of the Southern Ocean: Strong topographic effects and weak seasonality. *Deep*
1205 *Sea Res. Part Oceanogr. Res. Pap.* 57, 604–620. doi:10.1016/j.dsr.2010.01.004

1206 Park, Y.-H., Durand, I., Kestenare, E., Rougier, G., Zhou, M., d' Ovidio, F., Cotté, C., Lee, J.-H.,
1207 2014. Polar Front around the Kerguelen Islands: An up-to-date determination and associated
1208 circulation of surface/subsurface waters. *J. Geophys. Res. Oceans* 119, 6575–6592.
1209 doi:10.1002/2014JC010061

1210 Park, Y.-H., Roquet, F., Durand, I., Fuda, J.-L., 2008. Large-scale circulation over and around the
1211 Northern Kerguelen Plateau. *Deep Sea Res. Part II Top. Stud. Oceanogr.* 55, 566–581.
1212 doi:10.1016/j.dsr2.2007.12.030

1213 Parslow, J.S., Boyd, P.W., Rintoul, S.R., Griffiths, F.B., 2001. A persistent subsurface chlorophyll
1214 maximum in the Interpolar Frontal Zone south of Australia: Seasonal progression and
1215 implications for phytoplankton-light-nutrient interactions. *J. Geophys. Res. Oceans* 106,
1216 31543–31557. doi:10.1029/2000JC000322

1217 Pilskaln, C.H., Manganini, S.J., Trull, T.W., Armand, L., Howard, W., Asper, V.L., Massom, R.,
1218 2004. Geochemical particle fluxes in the Southern Indian Ocean seasonal ice zone: Prydz Bay
1219 region, East Antarctica. *Deep Sea Res. Part Oceanogr. Res. Pap.* 51, 307–332.
1220 doi:10.1016/j.dsr.2003.10.010

1221 Pinkerton, M.H., Smith, A.N.H., Raymond, B., Hosie, G.W., Sharp, B., Leathwick, J.R., Bradford-
1222 Grieve, J.M., 2010. Spatial and seasonal distribution of adult *Oithona similis* in the Southern
1223 Ocean: Predictions using boosted regression trees. *Deep Sea Res. Part Oceanogr. Res. Pap.* 57,
1224 469–485. doi:10.1016/j.dsr.2009.12.010

1225 Pollard, R., Lucas, M., Read, J., 2002. Physical controls on biogeochemical zonation in the Southern
1226 Ocean. *Deep Sea Res. Part II Top. Stud. Oceanogr.* 49, 3289–3305. doi:10.1016/S0967-
1227 0645(02)00084-X

1228 Primeau, F.W., Holzer, M., DeVries, T., 2013. Southern Ocean nutrient trapping and the efficiency of
1229 the biological pump. *J. Geophys. Res. Oceans* 118, 2547–2564. doi:10.1002/jgrc.20181

1230 Quéguiner, B., 2013. Iron fertilization and the structure of planktonic communities in high nutrient
1231 regions of the Southern Ocean. *Deep Sea Res. Part II Top. Stud. Oceanogr.* 90, 43–54.
1232 doi:10.1016/j.dsr2.2012.07.024

1233 Ragueneau, O., Savoye, N., Del Amo, Y., Cotten, J., Tardiveau, B., Leynaert, A., 2005. A new method
1234 for the measurement of biogenic silica in suspended matter of coastal waters: using Si:Al
1235 ratios to correct for the mineral interference. *Cont. Shelf Res.* 25, 697–710.
1236 doi:10.1016/j.csr.2004.09.017

1237 Ragueneau, O., Schultes, S., Bidle, K., Claquin, P., Moriceau, B., 2006. Si and C interactions in the
1238 world ocean: Importance of ecological processes and implications for the role of diatoms in
1239 the biological pump. *Glob. Biogeochem. Cycles* 20, GB4S02. doi:10.1029/2006GB002688

1240 Rembauville, M., Salter, I., Leblond, N., Gueneugues, A., Blain, S., 2014. Export fluxes in a naturally
1241 fertilized area of the Southern Ocean, the Kerguelen Plateau: seasonal dynamic reveals long
1242 lags and strong attenuation of particulate organic carbon flux (Part 1). *Biogeosciences Discuss*
1243 11, 17043–17087. doi:10.5194/bgd-11-17043-2014

1244 Richardson, K., Visser, A.W., Pedersen, F.B., 2000. Subsurface phytoplankton blooms fuel pelagic
1245 production in the North Sea. *J. Plankton Res.* 22, 1663–1671. doi:10.1093/plankt/22.9.1663

1246 Rigual-Hernández, A.S., Trull, T.W., Bray, S.G., Closset, I., Armand, L.K., 2015. Seasonal dynamics
1247 in diatom and particulate export fluxes to the deep sea in the Australian sector of the southern
1248 Antarctic Zone. *J. Mar. Syst.* 142, 62–74. doi:10.1016/j.jmarsys.2014.10.002

1249 Romero, O.E., Armand, L., 2010. Marine diatoms as indicators of modern changes in oceanographic
1250 conditions. In: 2nd Edition *The Diatoms: Applications for the Environmental and Earth*
1251 *Sciences.*, Camb. Univ. Press 373–400.

1252 Romero, O.E., Fischer, G., Lange, C.B., Wefer, G., 2000. Siliceous phytoplankton of the western
1253 equatorial Atlantic: sediment traps and surface sediments. *Deep Sea Res. Part II Top. Stud.*
1254 *Oceanogr.* 47, 1939–1959. doi:10.1016/S0967-0645(00)00012-6

1255 Romero, O.E., Lange, C.B., Fisher, G., Treppke, U.F., Wefer, G., 1999. Variability in export
1256 production documented by downward fluxes and species composition of marine planktonic
1257 diatoms: observations from the tropical and equatorial Atlantic., in: *The Use of Proxies in*
1258 *Paleoceanography, Examples from the South Atlantic.* Heidelberg, Berlin, pp. 365–392.

1259 Rynearson, T.A., Richardson, K., Lampitt, R.S., Sieracki, M.E., Poulton, A.J., Lyngsgaard, M.M.,
1260 Perry, M.J., 2013. Major contribution of diatom resting spores to vertical flux in the sub-polar
1261 North Atlantic. *Deep Sea Res. Part Oceanogr. Res. Pap.* 82, 60–71.
1262 doi:10.1016/j.dsr.2013.07.013

1263 Sackett, O., Armand, L., Beardall, J., Hill, R., Doblin, M., Connelly, C., Howes, J., Stuart, B., Ralph,
1264 P., Heraud, P., 2014. Taxon-specific responses of Southern Ocean diatoms to Fe enrichment

1265 revealed by synchrotron radiation FTIR microspectroscopy. *Biogeosciences* 11, 5795–5808.
1266 doi:10.5194/bg-11-5795-2014

1267 Sallée, J.-B., Matear, R.J., Rintoul, S.R., Lenton, A., 2012. Localized subduction of anthropogenic
1268 carbon dioxide in the Southern Hemisphere oceans. *Nat. Geosci.* 5, 579–584.
1269 doi:10.1038/ngeo1523

1270 Salter, I., Kemp, A.E.S., Moore, C.M., Lampitt, R.S., Wolff, G.A., Holtvoeth, J., 2012. Diatom resting
1271 spore ecology drives enhanced carbon export from a naturally iron-fertilized bloom in the
1272 Southern Ocean. *Glob. Biogeochem. Cycles* 26, GB1014. doi:10.1029/2010GB003977

1273 Salter, I., Lampitt, R.S., Sanders, R., Poulton, A., Kemp, A.E.S., Boorman, B., Saw, K., Pearce, R.,
1274 2007. Estimating carbon, silica and diatom export from a naturally fertilised phytoplankton
1275 bloom in the Southern Ocean using PELAGRA: A novel drifting sediment trap. *Deep Sea Res.*
1276 Part II Top. Stud. Oceanogr., The Crozet Natural Iron Bloom and Export Experiment
1277 CROZEX 54, 2233–2259. doi:10.1016/j.dsr2.2007.06.008

1278 Salter, I., Schiebel, R., Ziveri, P., Movellan, A., Lampitt, R., Wolff, G.A., 2014. Carbonate counter
1279 pump stimulated by natural iron fertilization in the Polar Frontal Zone. *Nat. Geosci.* 7, 885–
1280 889. doi:10.1038/ngeo2285

1281 Sancetta, C., 1995. Diatoms in the Gulf of California: Seasonal flux patterns and the sediment record
1282 for the last 15,000 years. *Paleoceanography* 10, 67–84. doi:10.1029/94PA02796

1283 Sanders, J.G., Cibik, S.J., 1985. Reduction of growth rate and resting spore formation in a marine
1284 diatom exposed to low levels of cadmium. *Mar. Environ. Res.* 16, 165–180.
1285 doi:10.1016/0141-1136(85)90136-9

1286 Sarmiento, J.L., Gruber, N., Brzezinski, M.A., Dunne, J.P., 2004. High-latitude controls of
1287 thermocline nutrients and low latitude biological productivity. *Nature* 427, 56–60.
1288 doi:10.1038/nature02127

1289 Schnack-Schiel, S.B., Isla, E., 2005. The role of zooplankton in the pelagic-benthic coupling of the
1290 Southern Ocean. *Sci. Mar.* 39–55.

1291 Smetacek, V., Assmy, P., Henjes, J., 2004. The role of grazing in structuring Southern Ocean pelagic
1292 ecosystems and biogeochemical cycles. *Antarct. Sci.* 16, 541–558.
1293 doi:10.1017/S0954102004002317

1294 Smetacek, V.S., 1985. Role of sinking in diatom life-history cycles: ecological, evolutionary and
1295 geological significance. *Mar. Biol.* 84, 239–251. doi:10.1007/BF00392493

1296 Steinberg, D.K., Goldthwait, S.A., Hansell, D.A., 2002. Zooplankton vertical migration and the active
1297 transport of dissolved organic and inorganic nitrogen in the Sargasso Sea. *Deep Sea Res. Part*
1298 *Oceanogr. Res. Pap.* 49, 1445–1461. doi:10.1016/S0967-0637(02)00037-7

1299 Suzuki, H., Sasaki, H., Fukuchi, M., 2001. Short-term variability in the flux of rapidly sinking
1300 particles in the Antarctic marginal ice zone. *Polar Biol.* 24, 697–705.
1301 doi:10.1007/s003000100271

1302 Suzuki, H., Sasaki, H., Fukuchi, M., 2003. Loss Processes of Sinking Fecal Pellets of Zooplankton in
1303 the Mesopelagic Layers of the Antarctic Marginal Ice Zone. *J. Oceanogr.* 59, 809–818.
1304 doi:10.1023/B:JOCE.0000009572.08048.0d

1305 Takahashi, T., Sweeney, C., Hales, B., Chipman, D., Newberger, T., Goddard, J., Iannuzzi, R.,
1306 Sutherland, S., 2012. The Changing Carbon Cycle in the Southern Ocean. *Oceanography* 25,
1307 26–37. doi:10.5670/oceanog.2012.71

1308 Takeda, S., 1998. Influence of iron availability on nutrient consumption ratio of diatoms in oceanic
1309 waters. *Nature* 393, 774–777. doi:10.1038/31674

1310 Tarling, G.A., Ward, P., Atkinson, A., Collins, M.A., Murphy, E.J., 2012. DISCOVERY 2010: Spatial
1311 and temporal variability in a dynamic polar ecosystem. *Deep Sea Res. Part II Top. Stud.*
1312 *Oceanogr.* 59–60, 1–13. doi:10.1016/j.dsr2.2011.10.001

1313 Taylor, S.R., McClenann, S.M., 1986. The continental crust: Its composition and evolution. *Geol. J.*
1314 21, 85–86. doi:10.1002/gj.3350210116

1315 Thomalla, S.J., Fauchereau, N., Swart, S., Monteiro, P.M.S., 2011. Regional scale characteristics of
1316 the seasonal cycle of chlorophyll in the Southern Ocean. *Biogeosciences* 8, 2849–2866.
1317 doi:10.5194/bg-8-2849-2011

1318 Treppke, U.F., Lange, C.B., Wefer, G., 1996. Vertical fluxes of diatoms and silicoflagellates in the
1319 eastern equatorial Atlantic, and their contribution to the sedimentary record. *Mar. Micropaleontol.* 28, 73–96. doi:10.1016/0377-8398(95)00046-1

1320 Uitz, J., Claustre, H., Griffiths, F.B., Ras, J., Garcia, N., Sandroni, V., 2009. A phytoplankton class-
1321 specific primary production model applied to the Kerguelen Islands region (Southern Ocean).
1322 *Deep Sea Res. Part Oceanogr. Res. Pap.* 56, 541–560. doi:10.1016/j.dsr.2008.11.006

1323 Venables, H., Moore, C.M., 2010. Phytoplankton and light limitation in the Southern Ocean: Learning
1324 from high-nutrient, high-chlorophyll areas. *J. Geophys. Res. Oceans* 115, C02015.
1325 doi:10.1029/2009JC005361

1326 Von Bodungen, B., Fischer, G., Nöthig, E.-M., Wefer, G., 1987. Sedimentation of krill faeces during
1327 spring development of phytoplankton in Bransfield Strait, Antarctica. *Mitt Geol Paläont Inst Univ Hambg. SCOPEUNEP Sonderbd* 62, 243–257.

1328 Weber, T.S., Deutsch, C., 2010. Ocean nutrient ratios governed by plankton biogeography. *Nature* 467, 550–554. doi:10.1038/nature09403

1329 Wefer, G., Fischer, G., 1991. Annual primary production and export flux in the Southern Ocean from
1330 sediment trap data. *Mar. Chem., Biochemistry and circulation of water masses in the Southern*
1331 *Ocean International Symposium* 35, 597–613. doi:10.1016/S0304-4203(09)90045-7

1332 Wefer, G., Fischer, G., Füetterer, D., Gersonde, R., 1988. Seasonal particle flux in the Bransfield
1333 Strait, Antarctica. *Deep Sea Res. Part Oceanogr. Res. Pap.* 35, 891–898. doi:10.1016/0198-
1334 0149(88)90066-0

1335 Wefer, G.G., Fisher, D.K., Futterer, R., Gersonde, R., Honjo, S., Ostermann, D., 1990. Particle
1336 sedimentation and productivity in Antarctic waters of the Atlantic sector., in: *Geological*
1337 *History of the Polar Oceans: Arctic versus Antarctic*. Kluwer Academic Publishers, The
1338 Netherlands, pp. 363–379.

1339 Westberry, T.K., Behrenfeld, M.J., Milligan, A.J., Doney, S.C., 2013. Retrospective satellite ocean
1340 color analysis of purposeful and natural ocean iron fertilization. *Deep Sea Res. Part Oceanogr.*
1341 *Res. Pap.* 73, 1–16. doi:10.1016/j.dsr.2012.11.010

1342 Wilson, S., E., Ruhl, H.A., Smith Jr, K.L., 2013. Zooplankton fecal pellet flux in the abyssal northeast
1343 Pacific: A 15 year time-series study. *Limnol. Oceanogr.* 58, 881–892.
1344 doi:10.4319/lo.2013.58.3.0881

1345 Wilson, S.E., Steinberg, D.K., Buesseler, K.O., 2008. Changes in fecal pellet characteristics with
1346 depth as indicators of zooplankton repackaging of particles in the mesopelagic zone of the
1347 subtropical and subarctic North Pacific Ocean. *Deep Sea Res. Part II Top. Stud. Oceanogr.* 55,
1348 1636–1647. doi:10.1016/j.dsr2.2008.04.019

1349 Wolff, E.W., Fischer, H., Fundel, F., Ruth, U., Twarloh, B., Littot, G.C., Mulvaney, R., Röthlisberger,
1350 R., de Angelis, M., Boutron, C.F., Hansson, M., Jonsell, U., Hutterli, M.A., Lambert, F.,
1351 Kaufmann, P., Stauffer, B., Stocker, T.F., Steffensen, J.P., Bigler, M., Siggaard-Andersen,
1352 M.L., Udisti, R., Becagli, S., Castellano, E., Severi, M., Wagenbach, D., Barbante, C.,
1353 Gabrielli, P., Gaspari, V., 2006. Southern Ocean sea-ice extent, productivity and iron flux over
1354 the past eight glacial cycles. *Nature* 440, 491–496. doi:10.1038/nature04614

1355 Yoon, W., Kim, S., Han, K., 2001. Morphology and sinking velocities of fecal pellets of copepod,
1356 molluscan, euphausiid, and salp taxa in the northeastern tropical Atlantic. *Mar. Biol.* 139,
1357 923–928. doi:10.1007/s002270100630

1358 Zielinski, U., Gersonde, R., 1997. Diatom distribution in Southern Ocean surface sediments (Atlantic
1359 sector): Implications for paleoenvironmental reconstructions. *Palaeogeogr. Palaeoclimatol.*
1360 *Palaeoecol.* 129, 213–250. doi:10.1016/S0031-0182(96)00130-7

1361

1362

1363

1364

1365 **Table 1.** Sediment trap cup collection dates, seasonal attribution, particulate organic carbon (POC)
 1366 and nitrogen (PON) fluxes, biogenic and lithogenic silicon (BSi and LSi) fluxes and molar ratios. POC
 1367 and PON data from Rembauville et al. (2014).

Cup	Cup opening date	Cup closing date	Collect ion time (days)	Season	Mass flux (mg m ⁻² d ⁻¹)	POC flux (mmol m ⁻² d ⁻¹)	PON flux (mmol m ⁻² d ⁻¹)	BSi Flux (mmol m ⁻² d ⁻¹)	LSi flux (μmol m ⁻² d ⁻¹)	% opal	POC:PON	BSi:POC
1	21/10/2011	04/11/2011	14	Spring	52.2	0.15	0.02	0.51	26.6	65.6	6.80	3.46
2	04/11/2011	18/11/2011	14	Spring	28.1	0.14	0.02	0.30	18.0	70.8	6.09	2.18
3	18/11/2011	02/12/2011	14	Spring	54.1	0.15	0.02	0.51	13.0	63.9	7.33	3.43
4	02/12/2011	12/12/2011	10	Summer	261.3	1.60	0.23	2.60	20.9	66.9	6.95	1.63
5	12/12/2011	22/12/2011	10	Summer	23.1	0.34	0.05	0.21	4.4	62.4	6.87	0.64
6	22/12/2011	01/01/2012	10	Summer	74.8	0.51	0.08	0.37	8.2	32.9	6.70	0.72
7	01/01/2012	11/01/2012	10	Summer	80.5	0.42	0.06	0.55	8.9	46.0	6.73	1.32
8	11/01/2012	25/01/2012	14	Summer	59.8	0.34	0.05	0.50	5.4	56.5	6.94	1.48
9	25/01/2012	08/02/2012	14	Summer	238.7	1.47	0.20	2.19	7.2	61.7	7.38	1.49
10	08/02/2012	22/02/2012	14	Summer	75.8	0.55	0.08	0.72	6.1	64.2	6.97	1.32
11	22/02/2012	31/05/2012	99	Autumn	24.4	0.27	0.03	0.08	1.5	21.5	8.09	0.29
12	31/05/2012	07/09/2012	99	Winter	5.1	0.04	0.01	0.03	2.2	35.0	6.06	0.66
Annual export (mmol m⁻² y⁻¹)					98.2	13.6	114	1.85				

1368

1369

1370

1371 **Table 2.** *Chaetoceros* resting spores (CRS) and *Thalassiosira antarctica* resting spores (TRS)
 1372 measurement and biomass data from station A3 sediment trap covering cups #4 (December
 1373 2011) to #11 (April 2012). For each variable, the range and the mean value (bold italic) is
 1374 reported.

Spore type	Number measured	Pervalvar axis (μm)	Apical axis (μm)	Shape *	Cell volume (μm^3)	Volume/Carbon relationship	Cell carbon content (pmolC cell $^{-1}$)	Cell carbon content (pgC cell $^{-1}$)
CRS	63	3.1 – 8.5 6	7.2 - 17.4 12.1	Cylinder + two cones	116.9 – 1415 483	0.039 pmolC μm^{-3} #	5 – 55 19	55 – 662 227
TRS	57	10.2 – 26 20.8	25.6 – 35.3 32.6	Cylinder + two half sphere	14035 – 48477 35502	$C = 10^{(0.811 \log_{10}(V)) - 0.541}$ §	56 – 153 119	672 – 1839 1428

1375 * As defined in Hillebrand et al., (1999)

1376 # Data representative of *Chaetoceros pseudocurvisetus* resting spore (Kuwata et al. 1993)

1377 § Equation from Menden-Deuer and Lessard, (2000), where C is the carbon content (pg C)
 1378 and V is the cell volume (μm^3)

1379

1380

1381 **Table 3.** Faecal pellet measurement and biomass estimations from Station A3 sediment trap.

1382 For each variable, the range and the mean value (bold italic) are reported.

Faecal pellet shape	Number measured	Major axis (μm) (a)	Minor axis (μm) (b)	Volume equation	Volume (μm^3)	Volume/carbon relationship	Faecal pellet carbon content ($\mu\text{molC pellet}^{-1}$)	Faecal pellet carbon content ($\mu\text{gC pellet}^{-1}$)
Spherical	4041	11 - 1069 150		$4/3 \pi (a/2)^3$	$697 - 6.39 \times 10^8$ 1.77×10^6		$2.09 \times 10^{-6} - 1.91$ 5.3×10^{-3}	$2.51 \times 10^{-5} - 23$ 0.06
Ovoid	2047	85 - 1132 314	10-802 154	$4/3 \pi (a/2) (b/2)^2$	$4.45 \times 10^3 - 3.81 \times 10^8$ 3.90×10^6	$0.036 \text{ mgC mm}^{-3} *$	$1.34 \times 10^{-5} - 1.14$ 11.7×10^{-3}	$1.60 \times 10^{-4} - 13.72$ 0.14
Cylindrical	1338	106 - 6152 981	14-547 136	$\pi (b/2)^2 a$	$1.63 \times 10^4 - 1.45 \times 10^9$ 1.43×10^7		$4.89 \times 10^{-4} - 4.35$ 0.04	$5.87 \times 10^{-4} - 52$ 0.51
Ellipsoid	54	301 - 3893 1329	51-1051 413	$4/3 \pi (a/2) (b/2)^2$	$4.10 \times 10^5 - 2.25 \times 10^9$ 1.19×10^8		$1.2 \times 10^{-3} - 6.75$ 0.36	0.01 - 81 4.28
Tabular	29					Constant, 119 $\mu\text{gC pellet}^{-1}$ #	9.92	119

1383 * Gonzalez and Smetacek, (1994)

1384 # Wilson et al. (2013)

1385

1386 **Table 4.** Full diatoms cells flux ($10^6 \text{ m}^{-2} \text{ d}^{-1}$) from the station A3 sediment trap. Full cells of
 1387 *Chaetoceros Hyalochaete* spp. were only found as resting spores.

Species – taxa group	Cup number												Contribution to annual flux (%)
	1	2	3	4	5	6	7	8	9	10	11	12	
<i>Asteromphalus</i> spp.	0	0.01	0	0.03	0	0	0	0	0.12	0	0	0	0.1
<i>Chaetoceros atlanticus</i> Cleve	0	0	0	0	0	0	0	0	0.07	0	0	0	0.0
<i>Chaetoceros atlanticus f. bulbosus</i> Ehrenberg	0	0	0	0	0	0	0	0	0	0	0	0	0.0
<i>Chaetoceros decipiens</i> Cleve	0	0	0.02	0	0	0	0	0	0.07	0	0	0	0.0
<i>Chaetoceros dichaeta</i> Ehrenberg	0	0	0	0.07	0	0	0	0	0.26	0	0	0	0.1
<i>Chaetoceros Hyalochaete</i> spp.	0.70	0	1.95	39.92	7.42	23.04	14.37	15.88	78.29	20.24	0.68	0	80.2
<i>Corethron inerme</i> Karsten	0	0	0	0	0	0	0	0	0.23	0	0	0	0.1
<i>Corethron pennatum</i> Grunow	0	0	0	0	0	0	0	0	0	0	0	0	0.0
<i>Dactyliosolen antarcticus</i> Castracane	0	0	0	0.05	0	0	0	0	0.02	0	0	0	0.0
<i>Eucampia antarctica</i> var. <i>antarctica</i> (Castracane) Mangin	0.08	0.03	0.06	0.19	0.08	0.36	0.19	0.65	1.03	0.45	0.08	0.01	1.6
<i>Fragilariopsis kerguelensis</i> (O'Meara) Hustedt	0.88	1.06	0	1.93	0.40	0.13	0.21	0.12	1.40	0	0	0	2.4
<i>Fragilariopsis separanda/rhomboica</i> group	0.02	0.16	0	0.68	0.05	0.20	0.13	0.07	1.47	0	0	0	1.1
<i>Guinardia cylindrus</i> (Cleve) Hasle	0	0	0	0	0	0	0	0	0.07	0	0	0	0.0
<i>Leptocylindrus</i> sp.	0	0	0	0.03	0	0	0	0	0	0	0	0	0.0
<i>Membraneis</i> spp.	0.04	0.01	0	0.19	0	0	0.02	0.02	0.02	0	0	0	0.1
<i>Navicula</i> spp.	0	0	0.04	0.64	0	0	0	0.29	0.58	0	0	0	0.6
<i>Odontella weissflogii</i> (Grunow) Grunow	0	0	0	0.08	0	0	0	0	0.05	0	0	0	0.0
<i>Pleurosigma</i> spp.	0.01	0	0	0.22	0.02	0.02	0	0.03	0.96	0.04	0	0	0.5
<i>Proboscia alata</i> (Brightwell) Sundröm	0	0	0	0	0	0	0	0	0.09	0	0	0	0.0
<i>Proboscia inermis</i> (Castracane) Jordan & Ligowski	0	0	0	0.03	0	0	0	0	0.33	0	0	0	0.2
<i>Proboscia truncata</i> (Karsten) Nöthig & Logowski	0	0	0	0	0	0	0	0	0	0	0	0	0.0
<i>Pseudo-nitzschia</i> spp.	0.26	0.02	0.21	1.81	0.08	0.45	1.85	1.56	7.08	0.36	0.02	0	5.6
<i>Rhizosolenia antennata/styliiformis</i> group	0	0	0	0	0	0	0	0	0.05	0	0	0	0.0
<i>Rhizosolenia chunii</i> Karsten	0	0	0	0	0.05	0	0	0.03	0.07	0	0	0	0.1
<i>Rhizosolenia crassa</i> Schimper in Karsten	0	0	0	0	0	0	0	0	0	0	0	0	0.0
<i>Rhizosolenia simplex</i> Karsten	0	0	0	0	0	0	0	0	0.07	0	0	0	0.0
<i>Thalassionema nitzschiooides</i> spp. Pergal & Pergal	1.45	1.48	0.20	4.65	0.28	0.14	0.34	0.72	0.89	0.14	0.05	0.01	4.0
<i>Thalassiosira lentiginosa</i> (Janisch) Fryxell	0.01	0	0	0	0	0	0	0	0	0	0	0	0.0
<i>Thalassiosira</i> spp.	0	0.05	0	0.05	0	0	0	0	0.12	0.05	0	0	0.1
<i>Thalassiosira antarctica</i> resting spore (TRS) Comber	0.04	0	2.19	2.65	0.17	0.14	0.13	0.14	0.12	0	0.01	0	2.1

<i>Thalassiothrix antarctica</i> Schimper ex Karsten	0	0	0	0.02	0.05	0.04	0.34	0.14	0.70	0	0	0	0.5
Small centrics (<20 μm)	0.05	0	0	0.41	0	0	0	0	0.19	0.18	0	0	0.3
Large centrics (>20 μm)	0	0	0.05	0.08	0	0	0	0	0.05	0	0	0	0.1
Total full cells	35.39	28.20	47.18	537.38	85.85	245.20	175.89	196.56	943.88	214.65	8.46	0.22	

1388

1389

<i>Thalassiothrix antarctica</i> Schimper ex Karsten	0	0	0	0	0	0.02	0	0	0	0.04	0	0	0.0
Small centrics (<20 µm)	0.48	0.44	2.96	16.87	0.28	0.13	0.17	0.24	0.65	0.20	0.03	0.02	15.7
Large centrics (>20 µm)	0	0.03	0.01	0.20	0	0	0	0	0.16	0.04	0	0	0.3
Total empty cells	8.34	3.28	10.57	61.20	1.12	1.59	3.01	4.43	28.98	5.46	0.59	0.07	

1392

1393

1394 **Table 6.** Total faecal pellet (FP) flux, total faecal pellet carbon flux, median volume and
 1395 carbon flux partitioned among faecal pellets types from station A3 sediment trap.
 1396 Contribution to numerical faecal pellet flux is provided in normal text whereas the
 1397 contribution to faecal pellet carbon flux is reported in bold italic.

Cup	Total FP flux (nb m ⁻² d ⁻¹) × 10 ³	Total FP carbon flux (mmol m ⁻² d ⁻¹)	Median volume (10 ⁶ µm ³)	Contribution (%)				
				Spherical	Ovoid	Cylindrical	Ellipsoid	Tabular
1	1.39	0.02	2.07	53.3 36.8	19.7 18.6	27.0 44.6	0.0 0.0	0.0 0.0
2	1.75	0.04	3.55	36.5 22.4	29.7 21.3	33.9 56.3	0.0 0.0	0.0 0.0
3	0.72	<0.01	0.95	62.7 54.5	37.3 45.5	0.0 0.0	0.0 0.0	0.0 0.0
4	21.81	0.48	1.91	76.4 83.1	22.8 15.3	0.8 1.6	0.0 0.0	0.0 0.0
5	5.10	0.12	3.71	26.6 13.8	35.0 18.3	38.3 67.4	0.1 0.5	0.0 0.0
6	2.69	0.15	5.67	28.8 4.6	33.1 10.9	37.9 43.1	0.0 0.0	0.2 41.3
7	2.46	0.12	6.71	15.6 2.5	45.5 16.1	37.1 56.0	1.8 25.3	0.0 0.0
8	2.06	0.20	6.18	37.6 1.9	15.5 2.1	44.2 34.6	2.2 15.8	0.4 45.5
9	1.36	0.09	3.59	40.4 2.8	20.5 4.9	35.4 27.9	3.7 64.4	0.0 0.0
10	1.22	0.03	2.34	56.0 17.7	22.4 9.1	21.3 69.9	0.4 3.3	0.0 0.0
11	0.27	0.13	2.10	38.9 0.4	30.8 0.7	20.3 2.5	5.7 3.9	4.3 92.6
12	0.14	0.06	2.41	18.4 0.4	57.6 2.6	20.3 5.3	0.0 0.0	3.7 91.8
Annually integrated contribution to faecal pellet flux				53.8 17.9	27.3 6.6	17.8 17.3	0.7 7.7	0.4 50.4

1398

1399

1400 **Table 7.** Measured and calculated POC fluxes, and POC flux partitioning among the major
 1401 identified ecological vectors of carbon exported out of the mixed layer at station A3.
 1402 Measured total POC flux from Rembauville et al. (2014). CRS: *Chaetoceros Hyalocahete*
 1403 resting spores, TRS: *Thalassiosira antarctica* resting spore.

Cup	Measured POC flux (mmol m ⁻² d ⁻¹)	Calculated POC flux (mmol m ⁻² d ⁻¹)	Contribution to calculated POC flux (%)								
			CRS	TRS	Other diatoms	Spherical faecal pellet	Ovoid faecal pellet	Cylindrical faecal pellet	Ellipsoid faecal pellet	Tabular faecal pellet	Total faecal pellet
1	0.15	0.05	25.3	8.1	38.6	10.3	5.2	12.5	0.0	0.0	28.0
2	0.14	0.06	0.0	0.0	35.4	14.5	13.7	36.4	0.0	0.0	64.6
3	0.15	0.31	12.1	85.1	1.4	0.8	0.6	0.0	0.0	0.0	1.4
4	1.60	1.62	46.8	19.4	3.9	24.8	4.6	0.5	0.0	0.0	29.8
5	0.34	0.29	48.0	6.9	3.3	5.8	7.7	28.2	0.2	0.0	41.8
6	0.51	0.63	69.7	2.7	3.2	1.1	2.7	10.5	0.0	10.1	24.4
7	0.42	0.43	63.1	3.5	5.8	0.7	4.4	15.4	7.0	0.0	27.5
8	0.34	0.56	54.4	2.9	6.8	0.7	0.8	12.4	5.7	16.3	35.9
9	1.47	1.71	86.8	0.8	7.2	0.1	0.3	1.4	3.3	0.0	5.2
10	0.55	0.44	88.1	0.0	4.3	1.4	0.7	5.4	0.3	0.0	7.7
11	0.27	0.14	9.1	1.2	2.2	0.3	0.6	2.2	3.4	81.0	87.5
12	0.04	0.06	0.0	0.0	0.5	0.4	2.6	5.2	0.0	91.3	99.5
Contribution to annual calculated POC flux (%)			52.1	8.6	5.0	5.1	2.0	5.2	2.2	19.8	34.3

1404

1405 **Figures captions.**

1406 **Figure 1.** a) Time series of the surface chlorophyll *a* concentration averaged in a 100 km
1407 radius around the trap location. The black line represents the climatology calculated for the
1408 period 1997/2013, whilst the green line corresponds to the sediment trap deployment period
1409 (2011/2012). b) POC fluxes (grey bars) and C/N molar ratio (red line) of the exported
1410 material, c) BSi flux (light blue bars) and BSi:POC ratio (blue line). Errorbars are standard
1411 deviation on triplicates.

1412 **Figure 2.** a) Total diatom cells fluxes (bars, left axis) and total empty:full cells ratio (blue
1413 line, right axis). b) to h) Fluxes of diatom cells from selected species identified as major
1414 contributors to diatom fluxes (>1 % of total diatom fluxes). In b), full cells are *Chaetoceros*
1415 *Hyalochaete* resting spores and empty cells are the vegetative stage. Full cell fluxes are
1416 represented by grey bars whereas empty cell fluxes are represented by white bars

1417 **Figure 3.** Factorial map constituted by the first two axes of the correspondence analysis
1418 performed on the full and empty diatom cell fluxes. Red squares are cup projections with cup
1419 numbers specified, blue circles are full cell projections, white circles are empty cell
1420 projections. The size of the markers is proportional to their representation quality in this
1421 factorial map.

1422 **Figure 4.** Annual ratio of empty to full cells for species observed as both forms. The dashed
1423 lines are the 0.5 and 2 ratio values. *Chaetoceros* *Hyalochaete* spp. full cells were only
1424 observed as resting spores.

1425 **Figure 5.** a) Faecal pellet numerical fluxes partitioned among faecal pellet types, b) boxplot
1426 of faecal pellet volume. On each box, the central mark is the median, the edges of the box are
1427 the first and third quartiles, the whiskers extend to the most extreme data points comprised in
1428 1.5 times the interquartile distance. c) faecal pellet carbon fluxes partitioned between the five

1429 faecal pellet types. The two arrows represent the two strong POC export events (cup #4 and
1430 #9, December 2011 and end January 2012, respectively).

1431 **Figure 6.** Heatmap representation of β correlation coefficients between the biological
1432 variables (empty and full-cell diatom and faecal pellet type fluxes) and the chemical variables
1433 (POC, PON, BSi, POC:PON and BSi:POC) resulting from the partial least square regression.
1434 Blue circles represent full diatom cells, white circles are empty diatom cells. Brown circles
1435 represent the faecal pellet type fluxes. The alphabetical labels within the symbols are used to
1436 identify the variable projections shown in Fig. 7. CRS: *Chaetoceros Hyalochaete* resting
1437 spores, TRS: *Thalassiosira antarctica* resting spores.

1438 **Figure 7.** Projection of the cups (red squares) the biological factors (circles) and the chemical
1439 factors (green diamonds) in the first two latent vectors of the partial least square regression.
1440 Circled labels refer to the full and empty species listed in Fig. 6.

1441 **Figure 8.** a) Grey bars in the background are measured POC fluxes, colored bars in the
1442 foreground are calculated POC fluxes partitioned among the main ecological vectors
1443 identified. b) Regression ($r^2 = 0.72$) between the measured and calculated POC fluxes. The
1444 correlation is highly significant (Spearman rank correlation, $n = 36$, $\rho = 0.84$, $p < 0.001$).
1445 Error bars were generated by increasing/decreasing the carbon/volume conversion factors by
1446 50 %. Black dashed line is the 1:1 relation, red line is the regression line, red dashed lines
1447 denotes the 99 % confidence interval. CRS: *Chaetoceros Hyalochaete* resting spores, TRS:
1448 *Thalassiosira antarctica* resting spores.

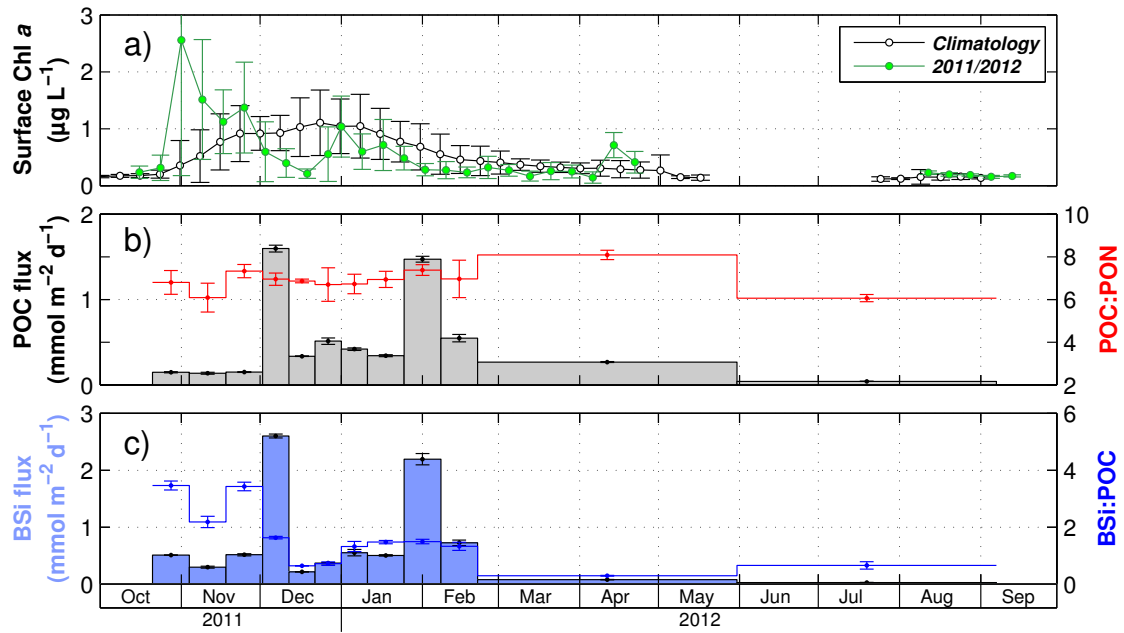


Figure 1.

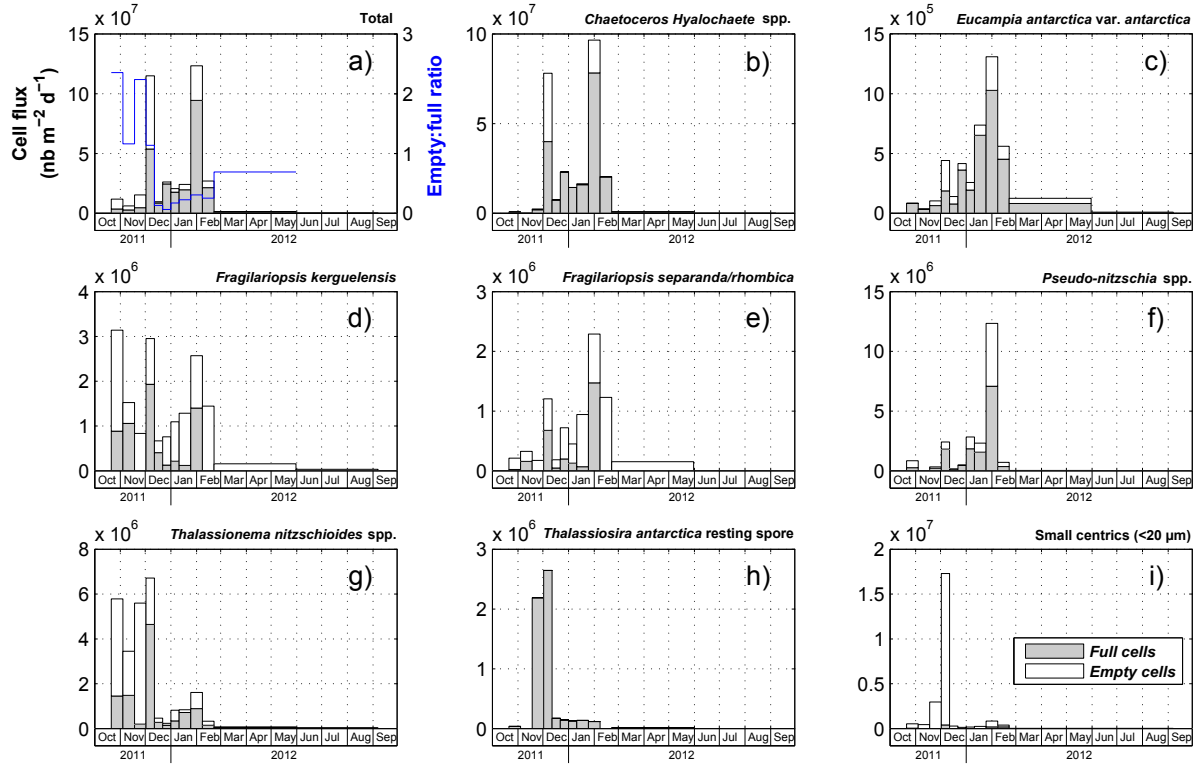


Figure 2.

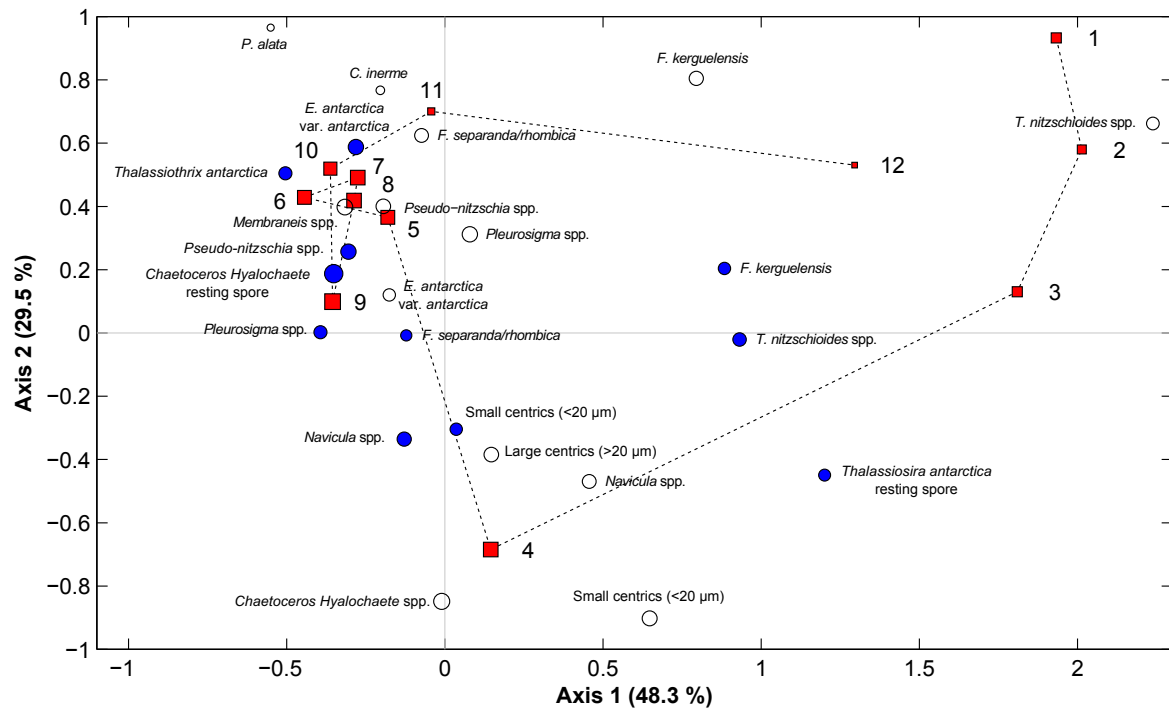


Figure 3.

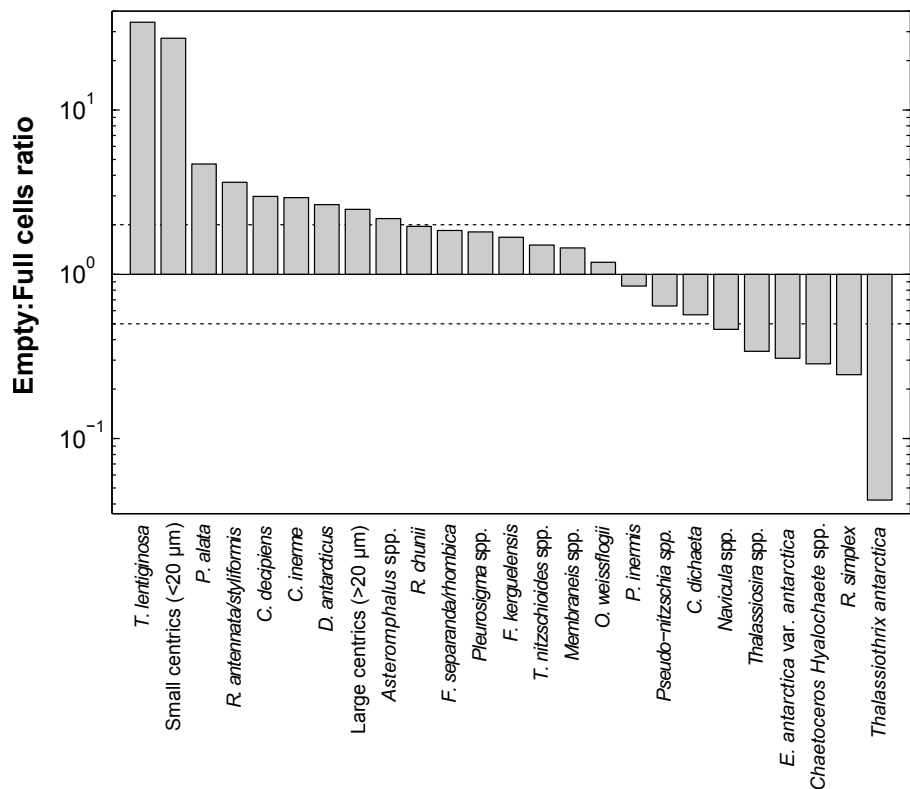


Figure 4.

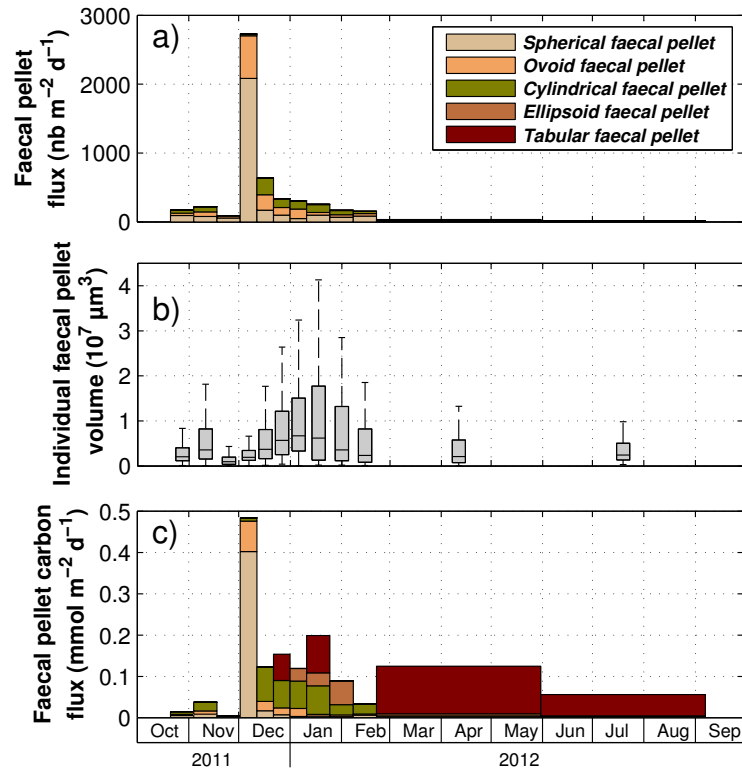


Figure 5.

	POC	PON	BSI	POC:PON	BSI:POC
CRS	0.07	0.07	0.06	0.02	-0.04
<i>E. antarctica</i>	0.05	0.05	0.03	0.02	-0.04
<i>F. kerguelensis</i>	0.05	0.05	0.07	0	0.07
<i>F. separanda/rhombica</i>	0.06	0.06	0.06	0.02	-0.01
<i>Navicula</i> spp.	0.07	0.07	0.07	0.02	0
<i>Pleurosigma</i> spp.	0.06	0.06	0.05	0.02	-0.01
<i>Pseudo-nitzschia</i> spp.	0.06	0.05	0.05	0.02	-0.01
<i>T. nitzschioides</i> spp.	0.04	0.04	0.06	0	0.07
TRS	0.03	0.03	0.05	-0.01	0.1
<i>Thalassiothrix antarctica</i>	0.04	0.04	0.03	0.01	-0.03
Small centrics (<20 μm)	0.06	0.06	0.07	0.01	0.01
<i>Chaetoceros</i> <i>Hyalochaete</i> spp.	0.07	0.07	0.07	0.02	0
<i>C. inerme</i>	0.03	0.03	0.02	0.01	-0.03
<i>E. antarctica</i>	0.08	0.07	0.06	0.02	-0.04
<i>F. kerguelensis</i>	0	0.01	0.05	-0.02	0.17
<i>F. separanda/rhombica</i>	0.04	0.04	0.03	0.01	-0.03
<i>Membraneis</i> spp.	0.06	0.06	0.05	0.02	-0.04
<i>Navicula</i> spp.	0.05	0.05	0.06	0.01	0.05
<i>Pleurosigma</i> spp.	0.06	0.06	0.06	0.01	0.01
<i>P. alata</i>	0.01	0.01	0	0.01	-0.03
<i>Pseudo-nitzschia</i> spp.	0.05	0.05	0.05	0.01	0
<i>T. nitzschioides</i> spp.	-0.03	-0.02	0.04	-0.04	0.24
<i>T. lenticinosa</i>	-0.04	-0.04	0.02	-0.04	0.22
Small centrics (<20 μm)	0.05	0.05	0.06	0.01	0.04
Large centrics (>20 μm)	0.07	0.07	0.07	0.02	0.01
Spherical faecal pellet	0.05	0.05	0.05	0.01	0.01
Ovoid faecal pellet	0.05	0.05	0.04	0.01	-0.02
Cylindrical faecal pellet	0	0	-0.02	0.01	-0.08
Ellipsoid faecal pellet	0.03	0.03	0.01	0.01	-0.06
Tabular faecal pellet	-0.01	-0.01	-0.05	0.02	-0.15

Figure 6.

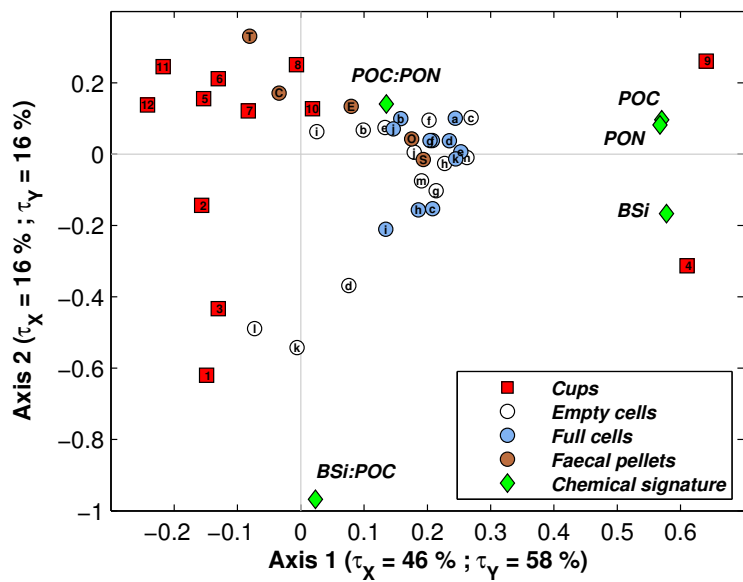


Figure 7.

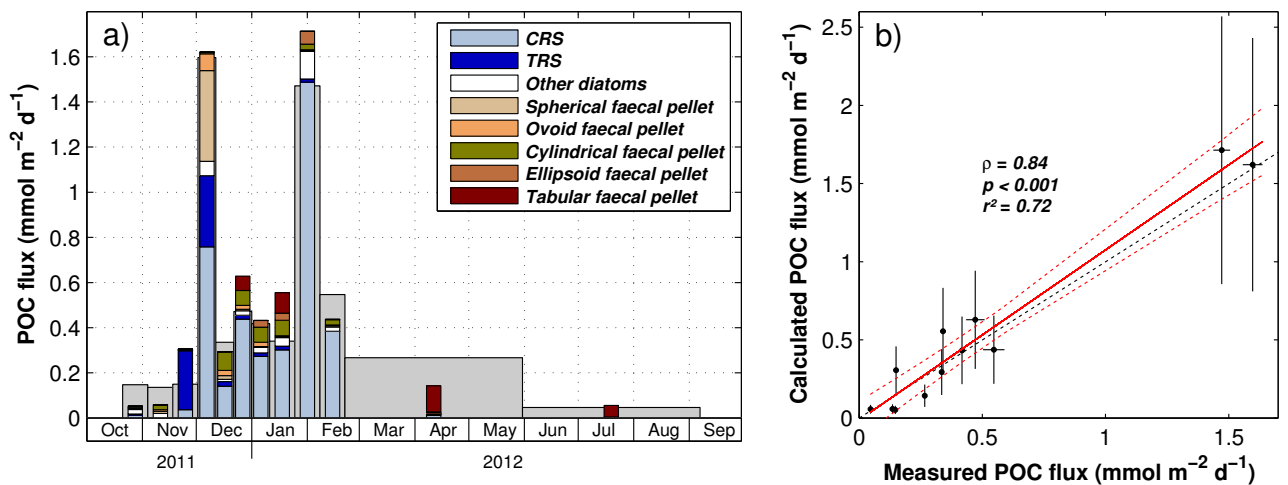


Figure 8.